A review of recent work on discharge characteristics during plasma electrolytic oxidation of various metals

Trevor William Clyne & Samuel Christopher Troughton

Published online: 26 Apr 2018.

Submit your article to this journal ⤤

Article views: 380

View Crossmark data ⤤

IoM³
The Institute of Materials,
Minerals and Mining

ASM
INTERNATIONAL

Taylor & Francis
Taylor & Francis Group

🔓 OPEN ACCESS | Check for updates

A review of recent work on discharge characteristics during plasma electrolytic oxidation of various metals

Trevor William Clyne 🄳 and Samuel Christopher Troughton 🄳

Department of Materials Science and Metallurgy, Cambridge University, Cambridge, UK

ABSTRACT

The review describes recent progress on understanding and quantification of the various phenomena that take place during plasma electrolytic oxidation, which is in increasing industrial use for production of protective coatings and other surface treatment purposes. A general overview of the process and some information about usage of these coatings are provided in the first part of the review. The focus is then on the dielectric breakdown that repeatedly occurs over the surface of the work-piece. These discharges are central to the process, since it is largely via the associated plasmas that oxidation of the substrate takes place and the coating is created. The details are complex, since the discharge characteristics are affected by a number of processing variables. The inter-relationships between electrical conditions, electrolyte composition, coating microstructure and rates of growth, which are linked via the characteristics of the discharges, have become clearer over recent years and these improvements in understanding are summarised here. There is considerable scope for more effective process control, with specific objectives in terms of coating performance and energy efficiency, and an attempt is made to identify key points that are likely to assist this.

1. Background to PEO processing

1.1. Historical development and range of metallic substrates

1.1.1. Introduction

Plasma electrolytic oxidation (PEO) processing allows the creation of durable, thick, uniform and strongly adherent coatings on metallic components of complex shape (including deep re-entrant features), without subjecting the substrate as a whole to elevated temperature and without requiring highly complex equipment. It also allows the creation of surfaces with a wide range of natural colours and textures. It thus has strong attractions for many applications. Industrial usage of PEO continues to increase and its study over recent years has become extensive. This can be seen from the publication statistics presented in Figure 1, which gives the number of papers published, and the citation levels for them, over the past 15 years. Furthermore, industrial and commercial exploitation of the process continues to expand. The current market leader, in terms of supply of PEO technology, is probably Keronite (UK), although activity is global, with available products including those from Ceratronic (France), Kepla-Coat/Magoxid-Coat (Germany) and Tagnite (U.S.A.). It seems likely that there will be major developments in the area over the next decade or two.

Nevertheless, understanding of the fundamentals of the process remains far from complete. It originated

from anodisation, in which the work-piece is placed in an electrolytic bath and a voltage (~10–80 V) is applied between it and an inert cathode. With certain metals, notably Al, Mg and Ti, an oxide film forms on the surface, often having a highly porous, fine columnar morphology (although other structures are possible [1,2]) and a fine-grained, and sometimes at least partially amorphous, atomic structure. The main features of anodising have been known for some time, with recent interest in the potential for its use to produce tailored nano-scale microstructures. Reviews and recent updates are available [3–6] covering the details of the process, including the variant of 'hard-anodising' [7,8] (in highly acidic electrolytes, sometimes with pulsing of the current).

In PEO processing (sometimes termed Micro-Arc Oxidation), higher voltages are employed (~250–750 V), usually in conjunction with an AC electrical supply, such that repeated dielectric breakdown occurs through the thickness of the growing oxide layer (during the anodic half-cycle), in the form of a large number of (micro)-discharges that are distributed over the surface of the work-piece. While the set-up and procedure appear nominally similar to anodisation, oxidation now takes place, not via continuous transport of ions through the electrolyte and within a thin oxide layer, but by a combination of metal and oxygen atoms or ions within the discharge plasma as it cools (the metal
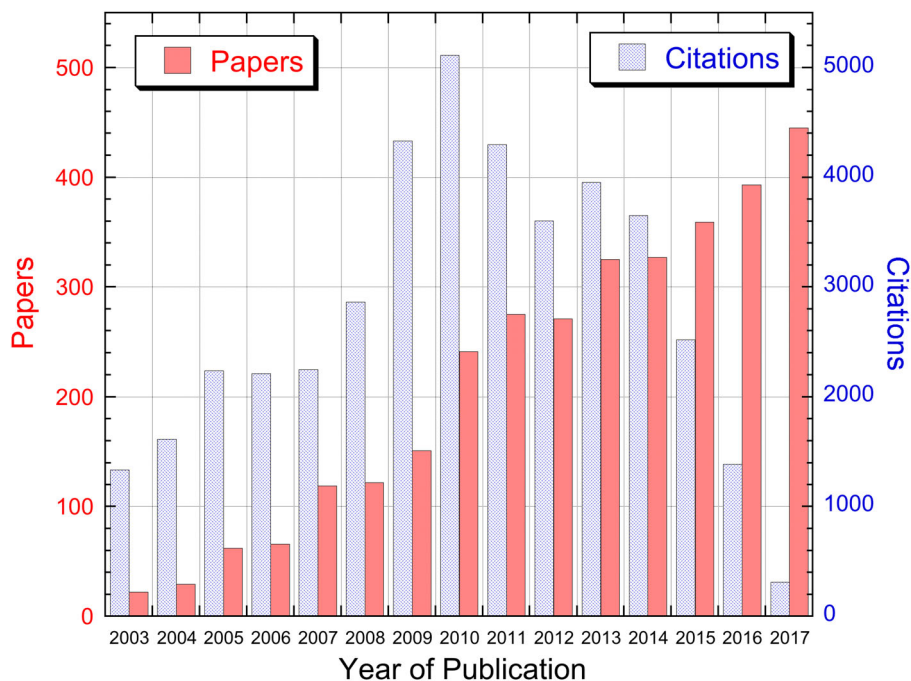
Figure 1. Publication data for PEO papers up to the end of 2017. Publication and citation data refer to the same papers, giving rise to the low citation numbers for very recent years. (These data are from the Web of Science, concerning papers containing the term 'Plasma Electrolytic Oxidation' or 'Micro-Arc Oxidation'.)

having entered the arc initially by evaporation from the substrate). This mechanism facilitates the production of thicker oxide layers and often results in a harder and more crystalline structure, mainly because discharges release large quantities of heat, tending to promote crystallisation in surrounding oxide material. In fact, PEO coatings do contain relatively high levels of porosity, with a complex architecture, but they tend to be more wear-resistant than anodised coatings, and they can in general also be grown to a greater thickness. This is limited only by the maximum thickness through which stable discharges can be generated, although it is well established that the voltage necessary for this does not rise in line with the macroscopic coating thickness and it is now clear that the actual dielectric breakdown occurs across a relatively thin oxide layer at the base of a deep pore in the coating.

It is clear that the PEO process is considerably more complex than anodising, and indeed than virtually all other coating procedures. One reason for this is that a PEO coating is being continually reconstructed throughout its thickness by the discharge formation that occurs while it is growing. Also, there is considerable scope for controlling the electrical and chemical conditions so as to modify the coating microstructure (via changes in the discharge characteristics and in the way that the oxidation and subsequent coating creation is taking place). Most of the control of this type that has been exercised in industrial practice has been carried out on a largely empirical basis. However, recent advances in understanding of the inter-relationships between processing conditions, discharge

characteristics and resultant coating microstructure have the potential for allowing more systematic control in the future. This review is focused on that objective, in the context of conventional PEO processing in aqueous electrolytes, although this first section largely presents fairly routine information that may be useful as background.

1.1.2. Range of metals and alloys used in PEO processing

PEO (and, indeed, anodising) is mainly focused on aluminium and magnesium alloys, for which it works well. It can, however, be applied to several other metals and there has in particular been a lot of work with titanium and its alloys. This has been largely because there is considerable interest in (highly porous) TiO_2 surfaces for certain types of application – mainly biomedical and photo-catalytic. In fact, it is difficult to produce thick (>~10–20 μm) PEO coatings on Ti and they often contain relatively coarse pores. There are other metals, making a total of about 7 or 8 (often collectively known as the 'valve metals' – see Section 'The "valve metals" and charge transfer during anodising and PEO' for an explanation of this terminology), for which PEO processing is regarded as routinely viable. These include Zr alloys, which have important applications in the nuclear industry and have been examined systematically in terms of suitability for PEO processing [9–12]. All of the valve metals have, as might be expected, highly stable oxides. However, while it is evident that this is not the only relevant characteristic, there is little clarity in the literature

about the specific set of properties that render a metal more or less suitable for PEO processing. The issue is addressed in some detail in the current review (Section 'Factors affecting the ease of discharge formation').

In addition to the features of a metallic element and its oxide(s) that affect the ease of PEO processing, there is interest in the role of alloying additions and the effect of the presence of second phase in alloy microstructures. In general, solute elements may become incorporated into the coating: (a) within the main oxide (i.e. it may become a mixed oxide), (b) as a separate oxide or (c) as some other kind of inclusion. Alternatively, these elements may end up in the electrolyte, either in solution or as solid suspensions. Some of these outcomes may have little or no effect on the progression of the PEO process, but others may start to cause problems in the form of an accumulation of species that inhibits the process in some way. For example, it is well established [13–15] that PEO of Al–Si (eutectic) alloys becomes inhibited after a while by accretion of the Si platelets, particularly in hyper-eutectic alloys [16]. On the other hand, metal matrix composites have been successfully PEO processed, with the ceramic reinforcement becoming incorporated in the coating. Examples include both magnesium [17] and aluminium [18] alloys containing SiC particulate.

It may be noted at this point that there is also the option, for metals unsuited to PEO processing (including steels and alloys of Ni, Cu, Sn, etc. – see Section 'Thermodynamics of oxidation during PEO'), of first plating them with a layer of a metal (such as Al) that is suitable and then producing the PEO coating (possibly consuming all of the plated metal). This has been explored in some detail, mostly for Al layers on steels [19–22]. It is in principle a viable and attractive option, but in practice there are problems. One is that, while electroplating is the most convenient option for production of such layers, this is inherently difficult for the metals that are most suitable for PEO (although it can be done). The main problem, however, is that there is a tendency to leave a residual (incompletely oxidised) aluminium layer and/or a poorly bonded interface between substrate and coating. This is unfortunate, since one of the inherent attractions of PEO is normally that there is very good substrate-coating adhesion. Nevertheless, the concept of a prior plating process remains an interesting one, with scope for a number of variants to be explored.

1.2. Processing conditions

1.2.1. Electrical conditions

A wide range of electrical conditions can be employed during PEO processing. While DC operation is possible, it has been repeatedly found that the process runs more effectively and the coatings are of higher quality when AC power supplies are used. These can be sinusoidal voltage supplies at 50 or 60 Hz (commonly used in laboratory and small-scale industrial settings), although square waveforms and higher frequencies are being increasingly exploited in research and in commercial use. Furthermore, a range of different electrical engineering control conditions can be used. It is common to set the current level (in both anodic and cathodic parts of the cycle), with the voltage adjusting to whatever is required to deliver these. However, there are other options, involving control over the capacitance in the system or over the applied voltage. These conditions naturally affect the characteristics of the discharges, and hence of the coatings. Effects of this type are described at various points in Section 'Discharge characteristics', but this review does not encompass detailed consideration of exactly how the electrical power supply can be controlled during PEO processing. Information of this type is available in the literature [23–26].

1.2.2. Electrolyte composition and additives

There is considerable scope for influencing the nature of the discharges, and of the resultant coating, by selection of the composition of the electrolyte. Sometimes the details of the compositions used are regarded as commercially sensitive, but in general PEO electrolytes are alkaline, commonly containing species such as KOH and Na_2SiO_3, and with pH values typically ranging up to about 13. It is not always entirely clear why a high pH is usually optimal for PEO, particularly since anodising is often carried out in acidic electrolytes. Furthermore, it is possible to perform PEO in acidic electrolytes, particularly for Ti [27–30]. It is certainly worth noting that (in both cases) the main mechanism of transport of oxygen towards the metal involves the movement of OH^- ions through the electrolyte, under the influence of an electric field. During anodising, however, there is just steady flow of ions along stable electrolyte channels, whereas in PEO the process is much more dynamic and transient. The electrolyte conductivity is also significant, since it affects current flow [31] and voltage drops across columns of electrolyte in pores within the coating, and can thus have an influence on the ignition of discharge plasmas [32,33]. This is examined in a little more detail in Section 'Electrolyte composition'. Conductivity values are commonly in the range 5–100 mS cm^{-1}.

It should be recognised, however, that a huge range of electrolyte compositions is in use, and that the potential influence extends beyond effects related to pH and conductivity. In particular, species in the electrolyte are likely to enter the discharge plasma, where they may influence the reactions that take place, and hence the nature of the substrate oxidation. It is also possible that species in the electrolyte could become incorporated into the coating via the plasma. This

can be done, for example, to control the colour of the coating – see Section 'Thermal and optical properties'. Many other effects have also been reported [28,34–38] concerning coating characteristics being influenced by additions to the electrolyte, although in the vast majority of cases these are simply empirical observations. It has also been noted [39] that 'aging' of electrolytes can influence the PEO process. This is, however, unsurprising, since there is considerable scope both for chemical changes to take place over time in unused electrolyte and, during use, for species from the substrate to enter the electrolyte in some form, with potential for contamination effects. It is common practice to use freshly prepared electrolytes where practicable, although clearly this can be difficult in an industrial environment.

Finally, it may be noted that there have been various attempts to incorporate additions such as fine particulate into PEO coatings, by adding them to the electrolyte. A review is available [40] concerning this type of measure. Depending on a number of factors (chemical, physical and electrical), particles may simply become physically entrapped in the coating as it grows or may undergo reactive incorporation. Some success has been reported [41–46] for such measures, although there will commonly be a danger that such dispersions are damaged or removed during the restructuring associated with repeated discharge formation. Nevertheless, it is clear that even very fine particulate can in some cases be successfully introduced into PEO coatings in this way. An example is provided in Section 'Photo-catalytic usage of Ti-based PEO coatings'.

1.3. Basic features of PEO discharges

1.3.1. Spectral analysis of PEO plasmas

There has been extensive study of the nature of the plasma created within PEO discharges, although their highly transient nature has made this a fairly complex undertaking. Plasma temperatures have been estimated [47–52] via optical spectroscopy to range from about 4000 to 12,000 K, with some indications of a higher temperature core and a lower temperature surrounding region. Corresponding electron densities typically range from $\sim 10^{15}$ to 10^{18} cm^{-3}.

It is also clear that PEO plasmas commonly contain many species, originating from the substrate, the existing coating and the electrolyte [50,53–56]. Of course, detailed results concerning the species present in the plasma, and their concentrations, depend on the compositions of substrate and electrolyte, and also on electrical conditions affecting the creation and nature of the plasma. It is certainly clear that relatively high concentrations of the substrate metal tend to be created in the plasma and it seems evident that the main oxide of the coating is formed in the plasma as it cools. This then condenses to a liquid, which becomes rapidly redistributed within the structure of the coating – see Section 'Redistribution of oxide after plasma collapse'.

1.3.2. 'Micro-discharge' characteristics

Typical discharges are now known [50,57–61] to occur in prolonged sequences ('cascades') at particular locations, and to have lifetimes of the order of a few tens to a few hundreds of microseconds, with 'incubation' periods between them of around a few hundred µs to a ms or two. The lifetime of a cascade can apparently be very long (perhaps of the order of a second or more [62]), although in practice during AC processing the discharges normally form only during the anodic part of the cycle, when the voltage is above a certain level, which limits the duration of a continuous sequence to something less than the half-cycle period – i.e. to several ms for a 50 Hz supply.

Discharge currents are typically several tens of mA, discharge energies a few mJ and diameters of core discharge channels a few tens of µm. Some correlations have been established [24,63–65] between external conditions, discharge characteristics and features of resultant coatings, including the coating growth rate, and progress has also been made [60,61,66] on correlating the energetics of individual discharges with that of the process as a whole (with the ultimate aim of reducing the – often relatively high – rate of energy consumption). Of course, the above figures are very approximate and the parameter values concerned are far from uniform during a given treatment and can also be quite sensitive to the processing conditions. Furthermore, the factors that control these parameters are not fully understood. Nevertheless, there have been important advances in understanding over the past decade or so and details of these are summarised later in this review.

1.4. Coating microstructure

1.4.1. Redistribution of oxide after plasma collapse

It is clear that at least most of the new oxide created during each discharge is formed within the plasma as it cools and collapses. This condenses as liquid, which is then injected into surrounding cavities under high local pressures, with some reaching the free surface, where it tends to erupt into 'volcanic craters', before solidification finally occurs. These features, examples of which are shown [67] in Figure 2, are characteristic of PEO coatings, although their size and distribution can vary substantially (typically becoming larger and more dispersed as the coating thickness increases). It is certainly evident from the appearance of these features that they are the result of liquid flow. Some authors have in the past suggested that the flow was initially of liquid metal, which
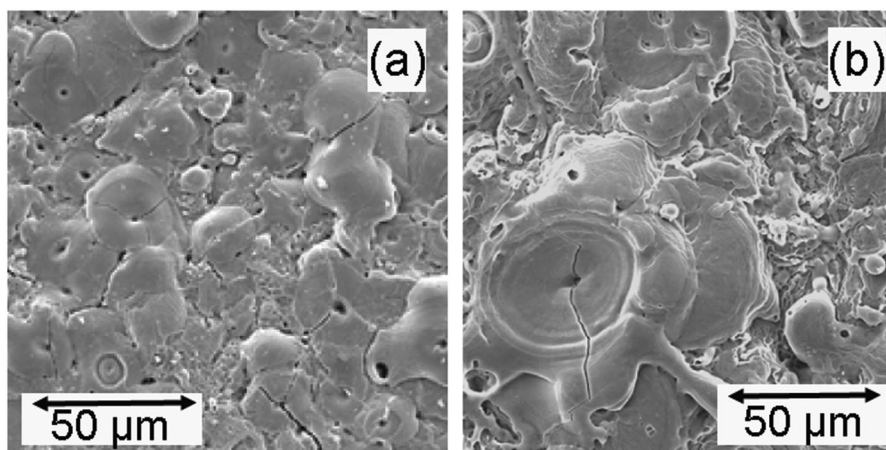
Figure 2. SEM micrographs [67] of typical free surfaces of PEO coatings (on Al), for coating thicknesses of (a) 5 μm and (b) 60 μm.

subsequently oxidised, but in fact it is now clear that it was already an oxide when it was flowing. Evidence for this includes the point that oxidation of metal would certainly change its appearance, so that it would no longer look like a 'frozen' liquid, and the fact that residual metal is never detected within a PEO coating. In any event, now that the sequence of events during PEO is better understood (see below), it is clear that the oxidation takes place before the structure of the coating has become established (during the cycle of individual discharges).

1.4.2. Phase constitution and grain structure

The microstructure of PEO coatings tends to be relatively complex. Local regions will have undergone very rapid solidification (quenched by the electrolyte after the most recent discharges), although regions in the immediate vicinity of those discharges may have effectively been heat treated (raised to fairly high temperature and then allowed to cool). In general, however, several features are observed that are characteristic of rapid solidification. These include a very fine grain structure (possibly close to, or actually, amorphous) and the presence of metastable phases. For Al, γ, η and ε, phases are sometimes present (although they are not easy to differentiate in XRD spectra), in addition to the stable α phase [68–70], while Ti PEO usually contains both anatase and rutile [71,72]. In both cases, amorphous material is often also present. Processing of the most common Ti alloy (Ti–6Al–4V) can generate [73,74] significant quantities of the mixed oxide $Al_2O_3 \cdot TiO_2$ (aluminium titanate). It is perhaps worth noting at this point that, in general, it is difficult to heat treat PEO coatings so as to modify these structures, since the range of temperature needed to effect significant change for such oxides would commonly be above, or at least close to, the melting temperature of the metallic substrate.

1.4.3. Porosity

Most PEO coatings are quite highly porous, with typical overall levels usually ∼10–20% for all substrates, having a complex architecture and covering a wide range of scales [75–77]. Almost all of the porosity is normally surface-connected. The reasons for the level and nature of this porosity are now clear, and are related to the way that the discharges form – see Section 'Discharge cascades and microstructural development'. Nevertheless, there are ongoing efforts to reduce these levels, or at least to make the porosity finer and more uniform [35,78,79]. Of course, it is true that coarse pores are likely to be deleterious. However, it should be appreciated that, on balance, the presence of the porosity in a PEO coating is beneficial in many cases. This is clear in the case of applications where a large specific surface area is required, such as for many biomedical and photo-catalytic purposes – see Sections 'Biomedical usage of PEO coatings' and 'Photo-catalytic usage of Ti-based PEO coatings'. Furthermore, PEO treatment is quite commonly employed in order to create a good keying surface for further surface treatment, such as painting. This is particularly the case for aluminium alloys and a recent review covers the issues in this area [80].

Slightly less obvious, but very important, are the mechanical stability benefits that arise from the effects of porosity (including microcracks) in a PEO coating in reducing its stiffness. This reduction is considerable, a typical change in Young's modulus compared with fully dense material being from ∼400 GPa to something of the order of 30–50 GPa in the case of PEO alumina [67,81]. This reduction strongly enhances the strain tolerance of the coating – for example, it reduces the stresses that arise if the component becomes deformed and also those due to differential thermal contraction with the substrate during thermal cycling. It may be noted at this point that it is the global stiffness of the coating that determines the macroscopic stresses generated in this way: the local stiffness, as obtained, for example,

by nanoindentation, will be much higher and might, depending on the indent size and the nearby distribution of pores, be close to the fully dense value.

1.4.4. Duplex, composite and graded PEO structures

Considerable effort has been devoted to the creation of PEO coatings with some kind of composite or graded structure. Clearly, there is scope for the creation of benefits. At a simple level, sealing of the surface in some way – for example, by the introduction of water glass via a sol–gel route – may lead to improved resistance to the entry of corrosive fluids (while retaining the mechanical benefits of interior porosity outlined in Section 'Phase constitution and grain structure'). Unfortunately, it is not easy to produce durable surface seals via a post-treatment of this type and there has been an extensive investigation into approaches to controlling the PEO process so as to create graded, duplex or hybrid structures within the coating. These have included gradients of phase constitution [82,83], incorporation of polymeric layers [84] and various kinds of composite coatings [85,86], as well as macroscopic structures such as metal-cored ceramic fibre networks [87]. In general, while these are all interesting possibilities, none have so far entered into mainstream usage.

1.5. Mechanical properties

1.5.1. Tribological characteristics

PEO coatings are attractive for many applications requiring resistance to sliding or abrasive wear. One reason for this is that they are highly resistant to spallation (partly because they adhere strongly to the substrate and partly because of their relatively low stiffness – see Section 'Phase constitution and grain structure'), so that the driving forces (strain energy release rates) for spallation tend to be low. Also important is the fact that, despite this low stiffness, they tend to be relatively hard – usually harder, for example, that anodised coatings, which often have a rather friable, columnar structure and contain a lot of amorphous material.

There has been a lot of work on optimisation of the wear resistance of PEO coatings [88–95], focusing on many different control variables, although the majority of such studies present empirical outcomes, rather than identifying the key microstructural features and the mechanisms by which they are being manipulated. Of course, wear is a complex phenomenon, and PEO is a complex process, so this is unsurprising.

1.5.2. Resistance to fatigue loading

In many cases, resistance to fatigue loading is dominated by the nucleation of cracks and the very early stages of crack growth. This usually occurs at the surface, so there is always interest in whether surface treatments or coatings are likely to enhance or impair the resistance to this type of damage development. Of course, corrosion may interact with mechanical fatigue processes. There has not been a huge amount of work in this area for PEO coatings, but concerns are often expressed about possible impairment of fatigue resistance. A possible mechanism for this is the removal (during PEO processing) of a surface layer of the metal that initially contained residual (compressive) stress – for example, from a shot peening operation. There are residual stresses in PEO coatings (see Section 'Residual stress levels'), and they are usually compressive, but they are relatively low (as would be expected of a porous layer that is being continually reconstructed), so this loss of compressive stresses in the original surface layer of the metal could cause degradation. Of course, this relates to fatigue testing without a pre-crack – i.e. it concerns the initiation of cracks, rather than their propagation. This is of direct industrial relevance and of course a coating is not expected to influence fatigue crack propagation in the bulk.

There are certainly reports [96–100] of significant impairment of fatigue life, for both Al and Mg alloys. There have been very few indications of any improvement, although it has been reported [101] that no change occurs with the Ti–6Al–4V alloy. It is thus certainly an area of concern. Possible explanations are not always forthcoming, but they usually focus either on residual stresses or on factors such as cracking in the coating, a roughened interface, or one where corrosion has occurred. It is certainly true that there can often be residual electrolyte left in a PEO coating. If this is not thoroughly flushed out with water (subsequently evaporated), then residues could be left that promote corrosion (particularly in moist atmospheres). Of course, such effects will be highly specific to the chemistry of the electrolyte and the corrosion conditions. The whole area of the fatigue resistance of samples with PEO coatings is one requiring further work.

1.5.3. Residual stress levels

An interesting point about PEO processing is that, since the coating is being continuously restructured by the discharges, it would be expected that any residual stresses created during the oxidation would tend to become repeatedly relaxed during this reconstruction. The relatively low stiffness of PEO coatings (Section 'Phase constitution and grain structure') will also tend to inhibit the generation of high stresses. Estimates based on information such as the volume change during oxidation (Pilling–Bedworth ratio), using handbook stiffness data, are therefore unlikely to be reliable.

In fact, there have been several reports [102–106] of high measured residual stress levels (>∼400 MPa) in

PEO coatings, although there are also very wide variations in the results. However, these were all obtained using measured shifts of X-ray diffraction peaks. This is not an easy technique to apply to PEO structures, which tend to have very fine grains, several different phases present and the potential for significant variations in composition. A macroscopic, global technique is likely to be preferable and indeed it has been shown via curvature measurements [81] that typical (compressive) stress levels in PEO coatings are around 50 MPa for Al and 150 MPa in Mg. Of course, all techniques for measurement of residual stresses are subject to some error, and the complex nature of PEO coatings tends to make these errors larger than in many other systems. Nevertheless, the broad experience is certainly that PEO coatings are strongly resistant to spallation and this is consistent with residual stress levels in them being low. Improved measurement and understanding of residual stresses in these coatings is an objective that merits further attention.

1.6. Environmental performance

1.6.1. Corrosion resistance

PEO coatings are commonly employed for the corrosion protection that they offer and there are many reports [45,107–109] of considerable enhancement. This is particularly true for Mg alloys [110–114], which are often very vulnerable to corrosive degradation without surface treatment. PEO coatings tend to adhere strongly, which is not the case for all coatings, perhaps particularly for an 'active' surface such as Mg. There are many examples of improved corrosion resistance being obtained via tailoring of electrolyte composition, so as to incorporate particular species in the coating, although such scenarios tend to be specific to the corrosive environment. Of course, it may also be beneficial to ensure that fluids cannot readily penetrate into the coating and various kinds of surface sealing operation are routinely employed.

1.6.2. Thermal and optical properties

There is considerable interest in controlling PEO so as to obtain modified thermal and optical properties. In particular, while materials like alumina are excellent thermal conductors as fully dense single crystals, the PEO structure (with very fine grains and extensive porosity) tends to confer a low conductivity (of the order of $1 \ W \ m^{-1} \ K^{-1}$). Since they can be quite thick (up to hundreds of microns in some cases), they therefore have potential as thermal barriers [115–117]. There have also been studies [118] of the thermal shock resistance of PEO coatings.

The optical properties that are most commonly of interest are those relating to absorption in the visible part of the spectrum, mainly since they determine the colour. It is well known that the PEO process is well suited to tailoring of conditions so as to control the colour of the coating. There are reports of conditions that generate colours of yellow [119], green [120], grey [121], red [122], blue [123] and black [124–126], among many others. There has also been work [127] on the reflection characteristics of PEO coatings in the IR part of the spectrum.

1.7. Functional characteristics

Extensive investigations have been carried out into the potential of PEO for generation of coatings with functional applications. The basis for much of this work has been exploitation of the high specific surface area of PEO coatings (due to their high porosity levels), primarily for Ti-based coatings. This is mainly because TiO_2 is known to be both highly bio-compatible (for bone ingrowth) and an effective photo-catalyst.

1.7.1. Biomedical usage of PEO coatings

Titanium is known to be a highly bio-compatible material, which means, of course, that it is titania that is biologically benign, since all titanium metal has a native oxide on the surface (normally one of the forms of TiO_2). In particular, bone cells have a high affinity with titania, and tend to grow into porous regions of it – or at least to adhere well to them and proliferate effectively on them. This is, of course, relevant to the production of strong bonding between (Ti alloy) implants and surrounding bone tissue. The idea that raising the specific surface area of the TiO_2 is likely to allow stronger bonding to the bone, by promoting a (porous) PEO layer on the surface, was first proposed some time ago. Moreover, the fact that some of the pores in PEO Ti are relatively coarse is actually beneficial in this situation, since bone cells have dimensions of the order of tens of microns and tend not to respond so well to very fine (sub-micron) porosity.

It has been shown in a number of studies [128–132] that these effects are significant, and that PEO surfaces do offer some promise in terms of biocompatibility. There are, of course, other options and alternative treatments, such as plasma spraying of hydroxyapatite onto Ti implants or surface patterning using mechanical or thermal methods, are currently more common in commercial practice.

There is also strong interest in Mg as a biomedical material [133]. Magnesium ions are in fact necessary for many biological processes in living cells, so that, in general, corrosion products are not inherently harmful. Additionally, the mechanical properties (particularly the density and Young's modulus) of Mg alloys are a closer match to bone than Ti alloys. However,

corrosion of Mg alloys can be very fast, generating excessive hydrogen and causing harmful local changes in pH. PEO coatings can be used to improve corrosion resistance, and can enhance biocompatibility by incorporating calcium and phosphorus from the electrolyte [134–138].

1.7.2. Photo-catalytic usage of Ti-based PEO coatings

Titania is known to be a very effective photo-catalyst – i.e. a surface on which oxidation of various organic pollutants and pathogens can take place readily under the action of suitable radiation [139]. It is common to use UV radiation, but certain measures, such as the introduction of Ag nanoparticles into the surface [140], allow longer wavelength (visible) radiation to be effective, raising the possibility of using sunlight as the radiation source. As with bioactivity, this has been known for a long time and the possibility of a Ti PEO surface being attractive (in view of its high specific surface area, and its potential for the creation of robust membrane structures) was proposed some time ago. There have been many investigations [141–147], with the potential now well established. Among relevant features is that the anatase phase is more effective than rutile [148] and there have been studies [149] in which efforts have been made to raise the anatase content of PEO coatings, with this effect in mind.

As with bio-compatible coatings, there are alternative ways of creating suitable surfaces and the PEO process is not yet in extensive commercial use for this purpose, although this may happen in due course. The objective of a high specific surface area is particularly important, although a pore architecture is required that facilitates fluid flow giving extensive exposure to the catalytic surface. For a membrane, this requires it to have a high permeability, which in turn is difficult to create if the pore structure is very fine. Furthermore, this must be combined with good penetration of the radiation to these surfaces. Such a combination is most easily achieved with a fine suspension of (TiO_2) nanoparticles in the fluid (commonly water), and indeed much research has been based on this approach. Unfortunately, it leaves the serious problem of how to remove this suspension after the treatment. Incorporation of a large number of such nanoparticles into the (relatively open) structure of a PEO coating is thus an attractive concept and it can be seen from Figure 3 that such material can be created.

2. Factors affecting the ease of discharge formation

2.1. Thermodynamics of oxidation during PEO

Clearly, the magnitude of the free energy change associated with a metal being converted to its oxide is relevant to PEO. This change is negative at ambient temperature for all metals (except gold), so oxidation is energetically favourable (at least at temperatures such that the metal is solid or liquid) in virtually all cases. However, as the plasma created during PEO
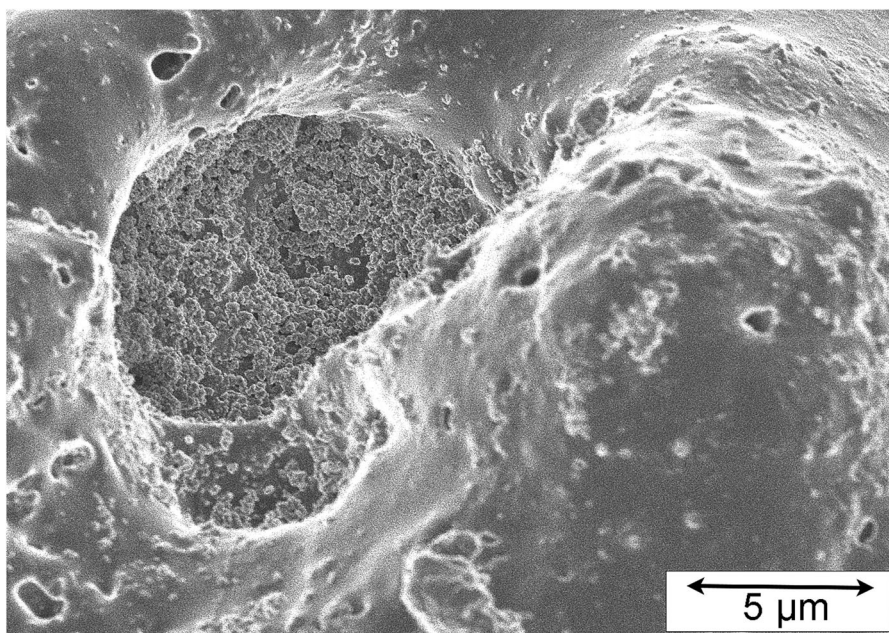

Figure 3. SEM micrograph (secondary electron image) of the free surface of a PEO coating produced on a Ti substrate, using a square-wave 50 Hz supply, anodic and cathodic voltages of 600 and 250 V and an electrolyte of 0.04 M sodium phosphate. The recess left of centre in this micrograph contains TiO_2 (anatase) nanoparticles, about 50–100 nm in diameter, which originated as a suspension in the electrolyte. (Image courtesy of Dr Mike Coto, of Keronite International and the Materials Science Department in Cambridge University.)
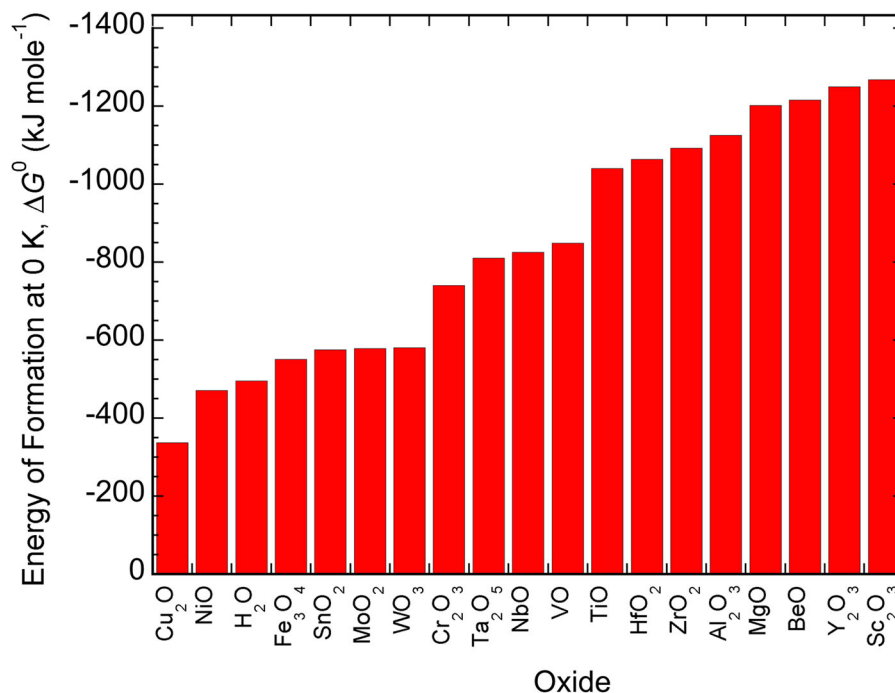
Figure 4. Free energy values [150,151] for the formation of various oxides from the metal, and of water from hydrogen, at 0 K. These energies are all expressed per mole of oxygen. For metals that can form more than one oxide, the data refer to the one for which the largest amount of energy is released.

collapses and cools, there may be competing oxidation reactions[1] for which the driving force is higher. In particular, the plasma is likely to contain hydrogen, so oxidation of metal ions (present as a result of volatilisation from the substrate) is only expected to take place to a significant extent if it is energetically more favoured than oxidation of hydrogen to form water.

Information of this type is provided by the Ellingham diagram for oxidation [150,151]. Some such data are shown in Figure 4, covering most of the metals of potential interest for PEO (excluding rare metals and others of limited interest, such as those that react strongly with water and very high atomic number elements). This graph actually shows only the enthalpy change (i.e. the free energy change at 0 K) associated with oxidation (per mole of oxygen). However, this is sufficient for (approximate) ranking purposes, since the rate of decrease of the magnitude of this energy change with increasing temperature is similar in most cases (reflecting the fact that much the same change in entropy occurs in each case, mainly due to a reduction in the number of moles of gas as the oxygen is consumed). It can be seen that, for metals with low energy changes (Cu, Ni, Fe, Sn, Mo and W), the driving force for oxidation is similar to, or lower than, that of hydrogen being converted to water. These metals are therefore unlikely to oxidise as a PEO plasma collapses and cools, particularly since the hydrogen

concentration there is likely to be relatively high. It is worth noting at this point that there are thus some very common types of metal (copper alloys, steels and Ni-based superalloys) that are expected to be unsuitable for PEO processing. In general, this is also what is found experimentally. There have been reports [152,153] of successful PEO processing to produce coatings on steels, but in such cases, it is probable that much of the oxide formation took place via deposition from the electrolyte, leading to friable and poorly bonded coatings. There is then a second group of metals (including Cr, Nb, Ta and V) for which the oxidation energy is higher than that for hydrogen, although not dramatically so. Finally, there is a third group (including Ti, Al, Mg, Be, Hf, Zr, Y and Sc) with very high values, such that there will clearly be a very strong thermodynamic driving force for oxidation.

Of course, this is a crude classification, and it must be borne in mind that the active oxidising agent in a PEO plasma as it cools is unlikely to be molecular oxygen, plus of course the temperature at which oxidation takes place is unknown (but will be relatively high) and the concentration of metal ions in it is also unknown (but will be relatively low). Data for the free energy changes under these conditions are simply not available. It should also be emphasised again that oxidation is not favoured for any metal at the temperatures

---

[1]It should be recognized that this is not a purely thermodynamic issue. Oxide formation can only occur when the plasma temperature has become relatively low (perhaps <∼3000 K, depending on the metal and its concentration) and at this point it is being rapidly quenched, perhaps passing through the temperature range concerned in a time as short as ∼10 μs. The kinetics of combination is therefore important. Of course, the presence of an excess of a competitor with a higher affinity for the oxygen, such as hydrogen in the case of some metals, will certainly slow down the kinetics of formation of the metal oxide and may inhibit it completely.

typical of these plasmas [154] and it is only towards the end of their collapse and cooling that combination with oxygen can occur. Nevertheless, it is relevant to observe that this last group contains the three metals (Al, Mg and Ti) that are most commonly (and successfully) subjected to PEO treatment. It might be noted that there is a common perception that Ti is not as easy to PEO process as the other two. Also, the oxide formed is invariably TiO_2, despite the fact that, according to the thermodynamic data, TiO is more stable (although there is some uncertainty about this issue, and more than one phase [155] with the approximate stoichiometry of TiO). Of the others in this group, there have been several reports [156–158] that Zr can be PEO processed. There appear to be no reports about PEO of Hf, Sc or Y, and very few [159] concerning Be, although it is sometimes included [160] in listings of metals that are suitable. (Of course, Be must be processed under highly controlled conditions, in view of toxicity problems.)

As mentioned above, it is fairly clear that metals such as Ni, Fe, Cu, Sn, Mo and W cannot normally be processed by PEO. Of course, it may be possible with heavily alloyed versions, such as NiTi shape memory alloy [161]. Also, the PEO conditions may have an influence and it has been shown [54] that Mo can be processed in an electrolyte of borax, water and ethylene glycol. (As mentioned in Section 'Introduction', this review is focused primarily on conventional PEO processing in aqueous electrolytes.) However, the metals put here into the central group (Cr, Nb, Ta and V) are of interest. Information about PEO of them is limited, although there have been reports of successful processing for both Nb [162–167] and Ta [29,168]. (Some further information about PEO of Ta is provided in Section 'PEO discharge characteristics for various metals'.) In any event, it is clear that, from a thermodynamic point of view, growth of the oxides of these metals should be possible, perhaps depending on their concentration, and that of hydrogen, in the plasma. This is certainly true for Ti, despite the fact that, as noted above, the perception is that, in practice, it is less suitable than Al and Mg. It therefore seems clear that there must be other factors affecting the ease of PEO processing.

2.2. The 'valve metals' and charge transfer during anodising and PEO

It is sometimes stated that PEO processing (and anodising) is applicable only to the 'valve metals' [169]. This terminology is not very well defined, but the concept is usually taken to mean that electrical current can only flow in one direction in the metal–oxide–electrolyte system [170]. The understanding is that electrons can flow through the oxide layer only when the metal is cathodic (i.e. in the direction metal to electrolyte). In the anodic half of the cycle, it is assumed that electrons cannot flow through the oxide, so the field across it builds up as the applied voltage is raised, and it may reach the breakdown level (dielectric strength) for the oxide, at which point a discharge occurs. This rectification effect is presumed to arise at the metal/oxide junction, across which electron flow can occur only from metal to oxide.

In fact, while there is a measure of agreement about the set that constitutes the valve metals – a list such as Al, Mg, Ti, Ta, Nb, Zr and Be is commonly quoted, it is quite certain that these could not have been identified from a knowledge of the rectification characteristics of the metal/metal oxide junctions concerned. Of course, depending on their band gap (see Section 'The band gap of the oxide'), many oxides can be regarded as semiconductors and such rectification (Schottky barriers) is exploited in various devices containing metal–semiconductor junctions. The sense of the rectification (i.e. whether electron flow can take place in the metal-to-semiconductor direction or in the reverse direction) is determined by the relative positions of the Fermi levels in the two constituents (and hence by the nature and level of the doping in the semiconductor). However, this approach evidently cannot be used to identify (or rationalise) the set of valve metals. Actually, most of the valve metal oxides have large band gaps (see Section 'The band gap of the oxide') and so cannot really be treated as semiconductors – and certainly not as (deliberately) doped semiconductors. This (increasingly outdated) approach to classifying metals as being suitable for PEO (or for anodising) is clearly flawed, although it does still get quoted on occasion.

On the other hand, there is certainly asymmetry, in the sense that PEO discharges usually (but not invariably – see Section 'Cathodic discharges and the effect of supply frequency') occur only during the anodic part of the cycle, and also that conventional anodising (oxidation) takes place only when the metal is made the anode. However, a more plausible explanation for this is that it arises because of asymmetry in what is taking place within the electrolyte with the two different polarities (and thus has at least some sensitivity to the electrolyte composition). This is illustrated in Figure 5, which gives a schematic depiction of the key steps during both anodising[2] and PEO (both polarities). For anodising, oxidation is expected to take place only when the metal is the anode, since

---

[2]Flow of ions through the oxide layer during anodization requires a very high field, and hence can only occur if it remains very thin (few nm). While it is common to depict this layer as if it has a significant thickness, it should be borne in mind that it must in fact be considerably thinner than the scale of the column structure.
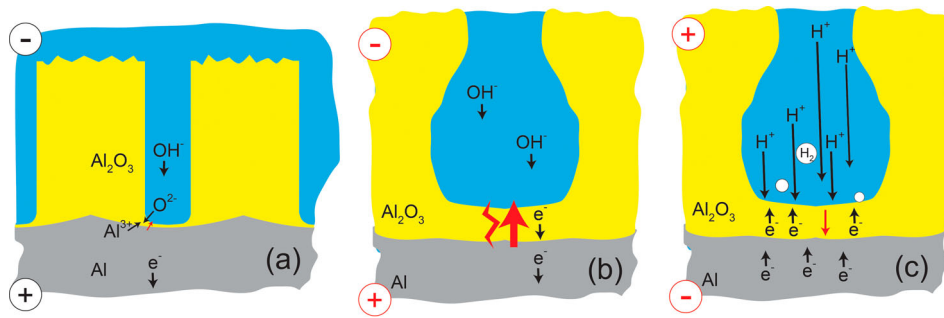
Figure 5. Schematic depictions of the transport phenomena taking place during (a) anodising, (b) PEO with anodic polarity and (c) PEO with cathodic polarity.

OH$^-$ ions will then reach it (through the electrolyte) and this is a source of the necessary oxygen. In fact, it is possible for anodisation to be carried out in acidic electrolytes (low OH$^-$ concentration) and there may in such cases be some breakdown of water molecules to release more oxygen. It is, of course, possible to predict the potential at which this will occur, for a given pH.

During PEO, on the other hand, oxidation of the metal takes place as the plasma collapses and cools, so the key issue is whether the electric field across the residual oxide layer reaches the level necessary for dielectric breakdown. It seems likely that the important point here is that, with anodic polarisation, the flow of electrons through the oxide is limited by the relatively slow rate of arrival of the OH$^-$ ions, which are moving through the electrolyte under the influence of the applied potential. This relatively slow rate of charge flow through the residual oxide layer ensures that the field across it reaches a level sufficient for discharge formation. Under cathodic polarity (Figure 5(c)), on the other hand, H$^+$ ions are attracted towards the oxide layer. These are much smaller and significantly more mobile than the OH$^-$ ions, allowing a greater rate of flow of electrons through the oxide layer, with hydrogen gas being released at its top surface. (In fact, the structure and dynamics of H$^+$ and OH$^-$ ions in aqueous solutions are quite complicated, with various complexes being formed [171], but nevertheless the outcome is understood to be that H$^+$ ions do move significantly more quickly under the influence of an electric field.)

Quantification of ionic motion in the electrolyte may be instructive and work on this is now starting [172]. This easier current flow in the cathodic half-cycle may limit the magnitude of the field across the oxide layer, reducing the likelihood of dielectric breakdown. It can be noted at this point that a sensitivity might be expected to the rate at which hydrogen ions combine to form molecules on the oxide surface: there are certainly variations in this catalytic efficiency between different surfaces (so that hydrogen evolution is said to be more or less strongly 'polarised' on different electrodes). This issue is addressed in Section 'Gas evolution'.

2.3. The band gap of the oxide

The oxides of most of the so-called valve metals have large band gaps. Broadly speaking, such band gaps (i.e. highly insulating oxides) might be expected to be associated with the oxide structure being highly stable thermodynamically, although there is not really a clear mechanistic link. Nevertheless, there is in practice a correlation, evident from the data [173] plotted in Figure 6, although it can be seen that it is not a close or well-defined one. (For example, the thermodynamic driving force for oxidation of Ti is similar to those of Al and Mg, but its oxide has a band gap with less than half the magnitude of those oxides.)

It is important to be clear about the relevance of the band gap to PEO processing. One issue is whether, treating the oxide as a semiconductor, it can acquire a relatively high electrical conductivity, either through doping or via thermal excitation of electrons across the band gap. In fact, the latter possibility can largely be ignored, since these layers remain cool (in contact with the electrolyte) up to the point of dielectric breakdown (and their band gaps are all very high compared with thermal energies). Extrinsic (doped) semiconducting behavior can also be largely neglected, since any such doping would be accidental and variable.

However, the issue of whether and how electrons can move through the oxide, and the relationship between this and the onset of dielectric breakdown, clearly is important for PEO and the band gap is significant in this respect. One possible mode of passage is electron tunnelling [174]. This is essentially a quantum effect and it is usually taken to be possible only through very thin layers – perhaps a few nm. It allows electrical contact to be established readily between nominally bare metal wires, even though they do in fact have (thin) surface oxide layers in the vast majority of cases.

The oxide layer thickness is clearly important and, while PEO coatings are often very thick (tens or hundreds of μm), it is now well established that residual oxide layers on the substrate remain much thinner throughout the process. This happens because PEO coatings are quite highly porous, particularly in the
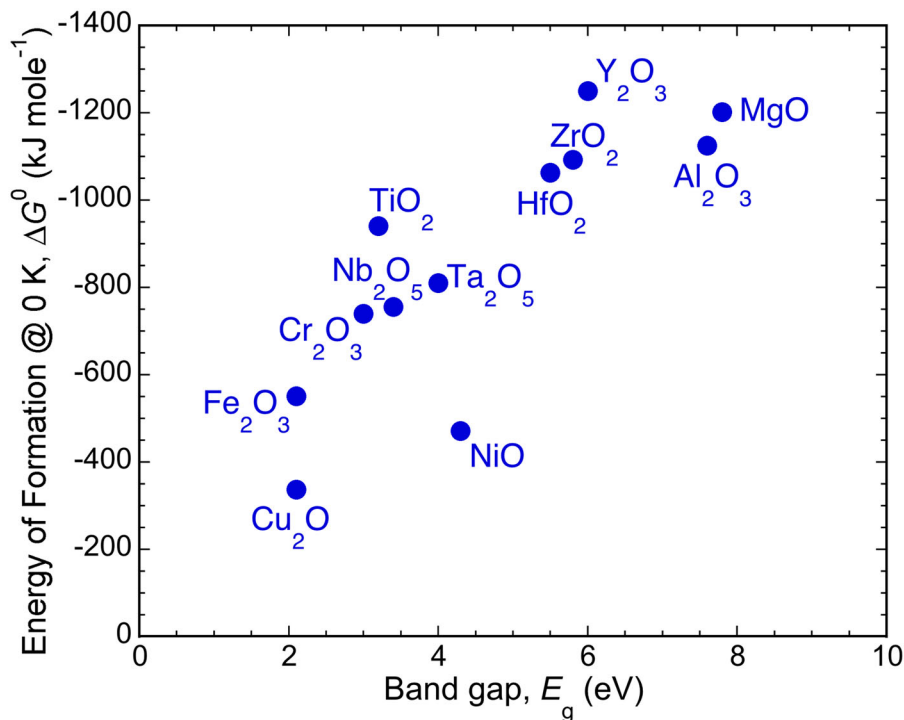
Figure 6. Plot of the free energy of formation of selected oxides against their band gap [173].

vicinity of an active discharge site, with the pores almost certainly being full of electrolyte before a discharge occurs – this is depicted in Figure 5(b,c). This explains the lack of any strong dependence on coating thickness of the voltage needed for PEO processing. In fact, while unequivocal evidence for this is lacking, there is a general consensus that dielectric breakdown commonly occurs during PEO across a residual oxide layer on the substrate that has a thickness of the order of 1 μm. (This issue is addressed in Section 'Discharge lifetimes, bubble growth and incubation times'.) While this is 'thin' for many purposes, it is probably too thick for electron tunnelling.

However, this does not mean that electrons cannot move through these oxides, and indeed it is well established that electron mobility can be relatively high in some oxides, particularly those with variable stoichiometry and high levels of various defects. Considered in terms of a band gap, such defects may provide energy levels within the gap, which assist motion of electrons through the material. A general correlation is still expected between a high band gap and a low electron mobility and, on this basis, the metals for which PEO can be carried out most readily are likely to have relatively large band gaps. The key point here is that, if electrons do travel through the oxide layer, this will not, in general, lead to any oxidation of the substrate, and it may carry much of the imposed current, so that PEO (i.e. plasma formation and oxidation within the plasma) may be reduced or eliminated (even though there may be a strong thermodynamic driving force for this oxidation). In such cases, the voltage during (the anodic half-cycle of) PEO is expected to

be lower than for cases in which most of the current is being carried by the discharges. Some support for this general idea is provided by the work of Munoz and Bessone [175], who showed that, during anodisation of Al, the introduction of small Ni and Co particles into the growing oxide layer (via cathodic deposition) raised the conductivity of the layer and hence reduced the electric field across it (and the rate of alumina growth).

2.4. Dielectric strengths and dielectric constants of oxides

The band gap evidently gives at least a pointer towards probable electron conductivity, and hence influences the electric field that tends to build up across the oxide. A dielectric strength is normally expressed as a breakdown field (in V m^{-1}), which is measured experimentally. The outcome of such experiments tends to be slightly variable, depending on factors such as the purity and porosity levels. For 'good' insulators, values are usually obtained which are above that of (dry) air (usually quoted as ~3 MV m^{-1}). Values for alumina and magnesia, for example, are usually in the range 10–30 MV m^{-1}. For other oxides, measurements have been made, often giving values in a lower range for oxides with smaller band gaps, but it is difficult to regard these as highly accurate or reliable and in general it is probably better to simply use band gap values (which are in most cases well established) as an indication of likely dielectric strength.

There is, however, another electrical property that is of potential significance here, which is the dielectric
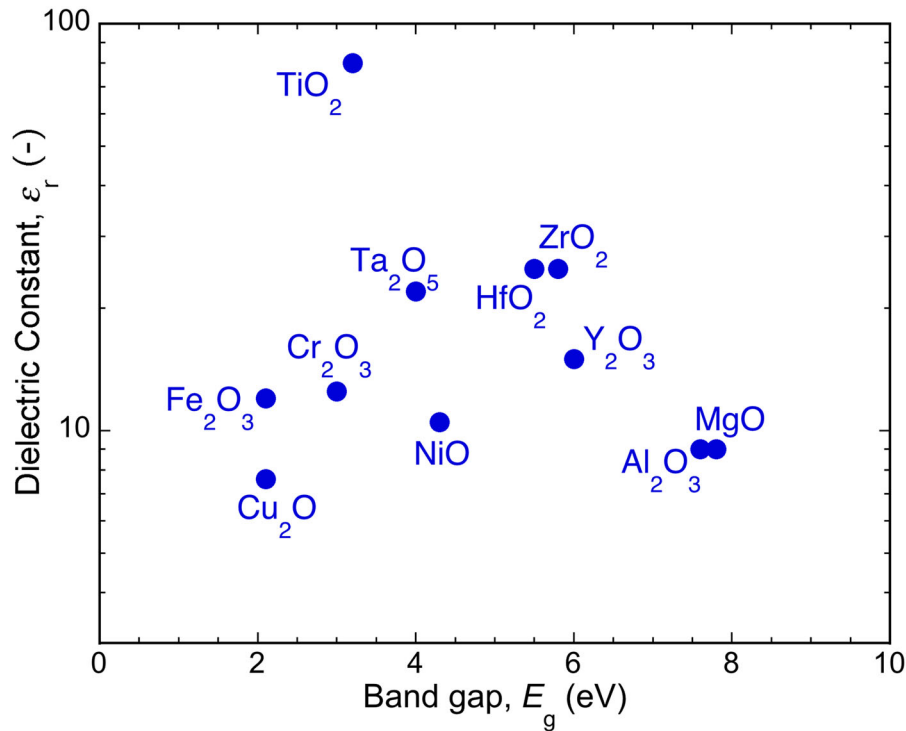
Figure 7. Plot of the dielectric constant [176] of selected oxides against their band gap.

constant (relative permittivity). This is a dimensionless number that gives an indication of the capacity of the lattice to store electric charge. It depends on the nature of the bonding (how strongly ionic it is) and on the arrangement of the ions. (Non-centro-symmetric structures can have very large dielectric constants.) The exact significance of this for PEO is not clear, but the capacity of the oxide to store charge may affect the electric fields being created during the process (under AC conditions). There is no obvious reason why its value should correlate with either the band gap or the thermodynamic stability and indeed the plot shown in Figure 7 suggests that there is no clear correlation. It may be noteworthy that TiO$_2$ has a very high dielectric constant – note the log scale in this plot.

2.5. Electrolyte composition

The electrolyte clearly fulfils several functions, as outlined in Section 'Electrolyte composition and additives'. Primarily, it allows electric charge to flow around a circuit, so its electrical conductivity is relevant. It is also clear that the pH can be important and that, at least in some cases, species in the electrolyte may become incorporated into the coating and/or influence its microstructure and properties. Regarding ease of discharge formation, there is a shortage of systematic information about the role of electrolyte composition, but there have been a few studies dedicated to this. For example, Figure 8 shows the breakdown voltage [177] as a function of electrolyte concentration (three different types of solution) during processing of an Mg alloy. (These data actually relate to a DC voltage,

and could thus be regarded as information about termination of an anodisation procedure, but this is in the context of PEO studies.) It can be seen that this voltage falls considerably as the concentration (and hence the conductivity) of the electrolyte is raised. This presumably relates to a part of the applied potential dropping across the electrolyte, leaving less to create the (breakdown) field across the oxide layer. There have been a number of studies, over an extended period [32,33,178,179], that are relevant to this issue.

Calculations can be made concerning this potential drop effect, using electrolyte conductivity data. On the scale of the complete set-up, these are complicated by convection etc., but simple estimates can be made relating to the potential drop across a (stagnant) column of liquid within the pore above a PEO discharge site. The variables involved, apart from electrolyte conductivity, σ, are the dimensions of the pore (height h and diameter D) and the (discharge) current, I. The voltage drop is then given by

$$\Delta V = \frac{4hI}{\pi D^2 \sigma} \qquad (1)$$

A plot of this function is shown in Figure 9, using variable values broadly appropriate for thick and thin PEO coatings (and a current value typical of the 'baseline' value before a discharge). The curves suggest that significant drops (>∼ few tens of V) may be common, implying in turn that the electrolyte conductivity (within the range commonly employed) can have a noticeable effect on electrical characteristics of discharges. This is an area in which more detailed work may be worthwhile.
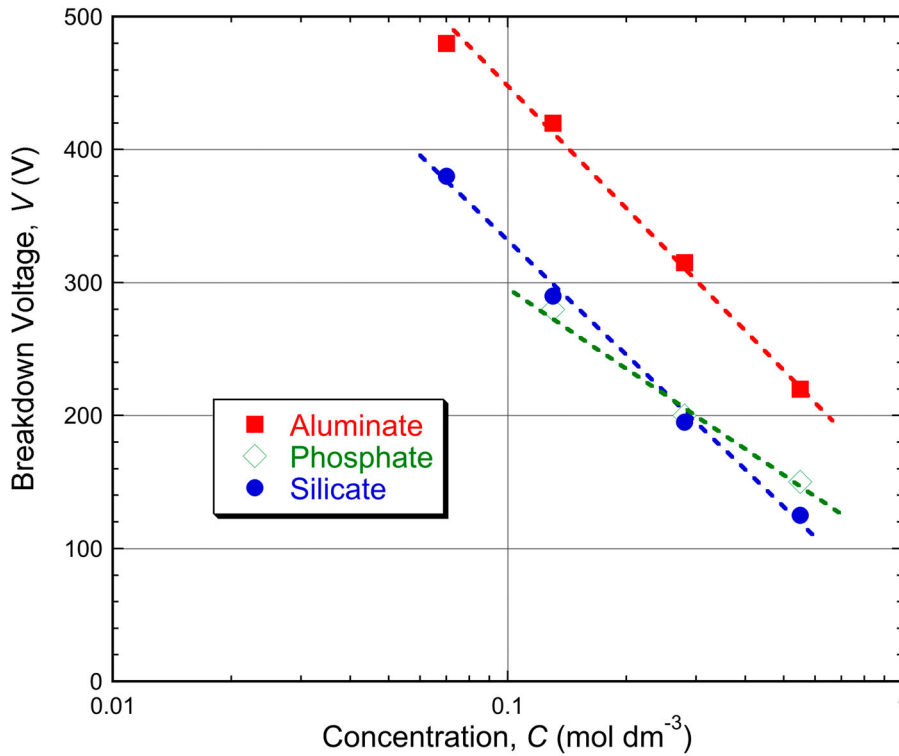
Figure 8. Plot [177] of the breakdown voltage during anodisation, as a function of the type and concentration of the electrolyte.

3. Discharge characteristics

3.1. Small area sample monitoring of currents in individual discharges

The key, indeed the defining, characteristic of PEO is the repeated formation of discharges on the surface of the sample, within which the substrate metal is converted to oxide. The nature of these discharges and their distributions in time and position are thus central to understanding and control of the process. This understanding has been advanced considerably as a result of the development of the small area sample
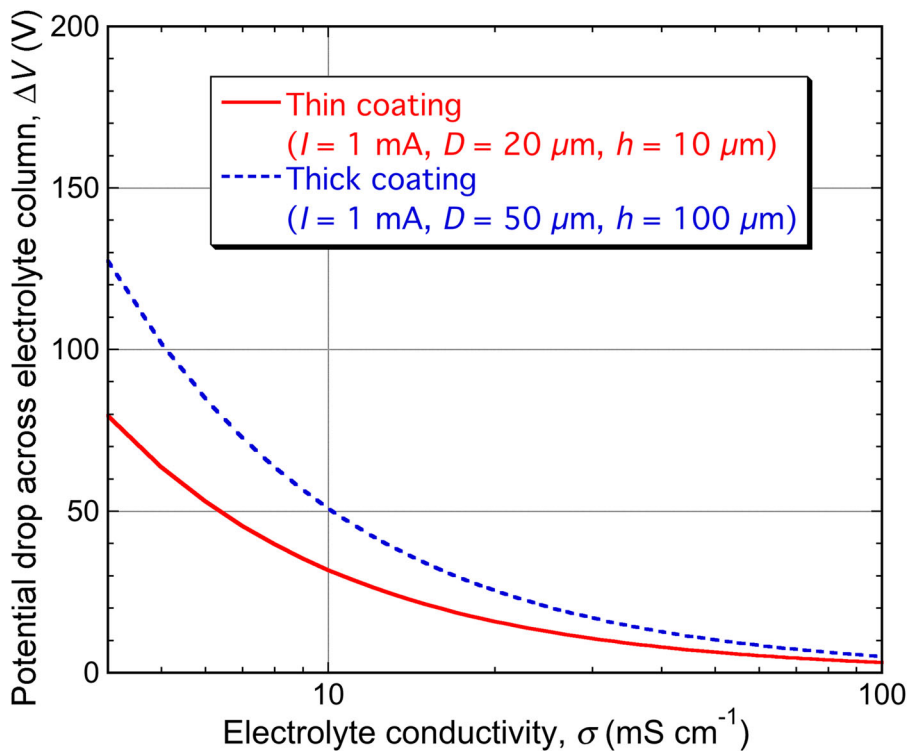

Figure 9. Curves showing the voltage drop across a cylindrical electrolyte column, using Equation (1) in combination with input data appropriate for PEO coatings immediately before a discharge.
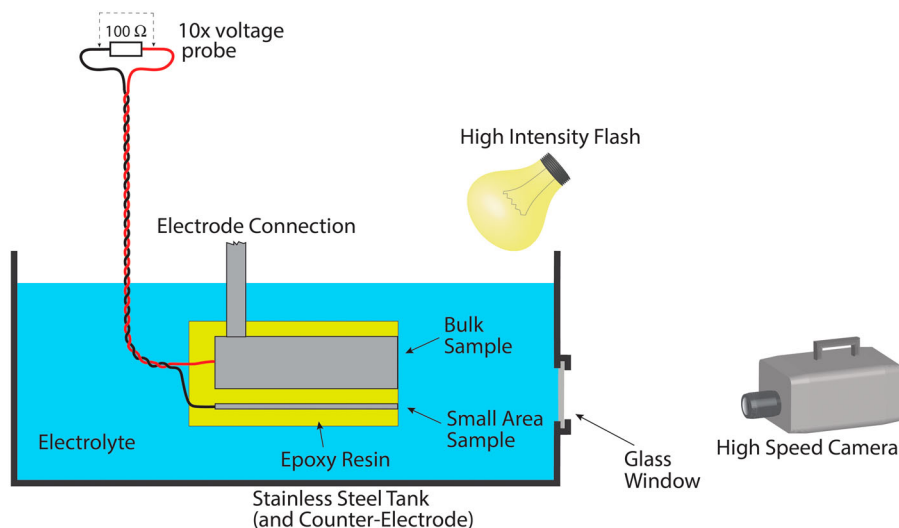
Figure 10. Schematic depiction of a small area sample set-up for monitoring of electrical and optical characteristics of individual discharges during PEO.

technique (by Dunleavy co-workers [50,57,59], based on the earlier work by Klein and co-workers [180,181]). The concept is illustrated in Figure 10, which shows the experimental arrangement. This allows the current through the small area sample to be continuously recorded (typically at rates of up to about 1 MHz), while obtaining synchronised optical information, either from the light emitted by the discharges or via high-intensity (short duration) illumination.

The central idea is that, provided the area of the small sample is sufficiently small, only single discharges will be occurring on it at any given time. Parallel processing of a conventional (bulk) sample, where many discharges are taking place throughout, ensures that, overall, the PEO process is proceeding as normal. The current associated with individual discharges (taking place on the small sample) can thus be monitored, and also correlated with optical emissions. The voltage, which is acting similarly on both small and large samples, is monitored in a conventional way (also synchronised with the small area current), as is the overall current. In detail, there may be some uncertainties about the exact similarity of conditions between small area and conventional conditions – for example, the electric field is probably more divergent for the small area sample, there may be an uncertainty about its exact surface area and in some cases more than one discharge (cascade) could be taking place on it at the same time. Nevertheless, in general the technique is clearly capable of revealing important information that is relevant to conditions during conventional processing of bulk samples.

There is no doubt that current pulses associated with individual discharges can be captured using this approach. For example, Figure 11 shows a result from early work [50], in the form of synchronised plots of current and light emission intensity – in this case for DC processing of an isolated small area Al sample. It is clear that the pulses of both light emission and current coincide closely with the occurrence of discharges. It can be seen that in this case the current pulses reached about 30–40 mA.

Later work has focused on AC conditions, with small area samples being processed in parallel with bulk material. Typical variations [62] of voltage and (small area) current are shown in Figure 12, for 50 Hz (square wave) processing of Al. It can be seen that seven discharges occurred during this particular anodic half-cycle (10 ms period). The anodic voltage developed was about 600 V. The average current during this cycle was about 20 mA. Discharges did not occur during every half-cycle and the overall average anodic current was about half of this value. It can be seen that at least most of the current is being carried via the discharges – a simple estimate leads to a value of over 80%.

The average current during the cathodic half-cycles is more homogeneous and was also ∼10 mA, although it can be seen that the voltage needed to create this was only ∼150 V. This lower voltage in the cathodic half-cycle is consistent with the arguments put forward in Section 'The "valve metals" and charge transfer during anodising and PEO' (Figure 5) about the higher mobility of hydrogen ions allowing easier charge transfer through the electrolyte. No discharges took place during the cathodic half-cycles (although they can occur under some circumstances – see Section 'Cathodic discharges and the effect of supply frequency').

Converted to a current density, using the nominal surface area of the wire, a current of 10 mA corresponds to about 200 A dm^{-2}, which is larger by a factor of about 6 than the pre-set value (which flows through the bulk sample). This difference is partly attributed to the convergent nature of the electric field in the vicinity
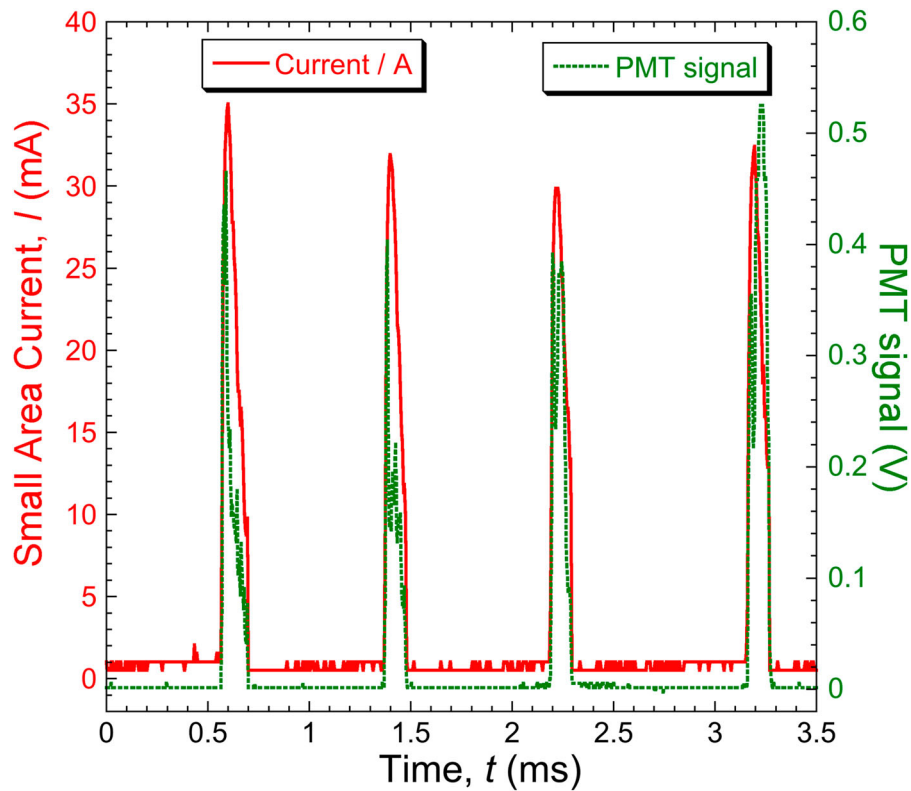
Figure 11. Typical data [50] showing a sequence of current pulses, and associated light emissions captured by a photomultiplier tube (PMT), during small area DC processing of an Al alloy.
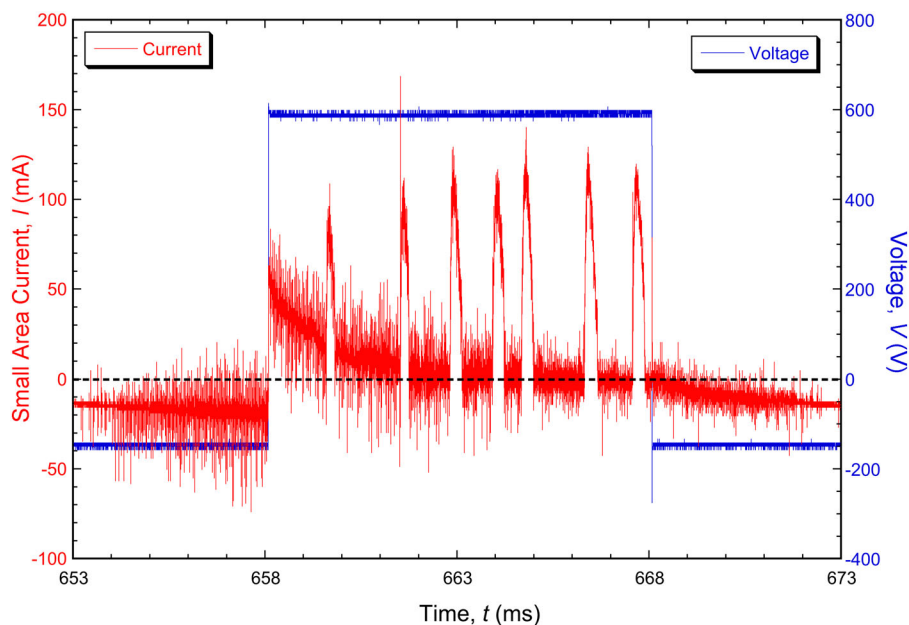

Figure 12. Synchronised plots [62] of voltage and (small area) current during PEO of Al-2014 alloy with a (square wave) 50 Hz supply. The coating thickness at this point was about 100 μm.

of the small area sample (analogous to the 'corner effect' often observed with bulk samples) and also to some coating production on the cylindrical surface of the wire exposed by the small interfacial gap between it and the surrounding resin. It can be seen that typical peak discharge currents were ~100 mA and discharge lifetimes were ~300 μs, with 'incubation periods' between them of the order of 1–2 ms.

3.2. Discharge cascades and microstructural development

An important feature of PEO is that these discharge sequences have a strong tendency to occur repeatedly at particular locations on the surface of the sample – i.e. they occur in 'cascades' that typically consist of hundreds, or even thousands, of individual discharges.
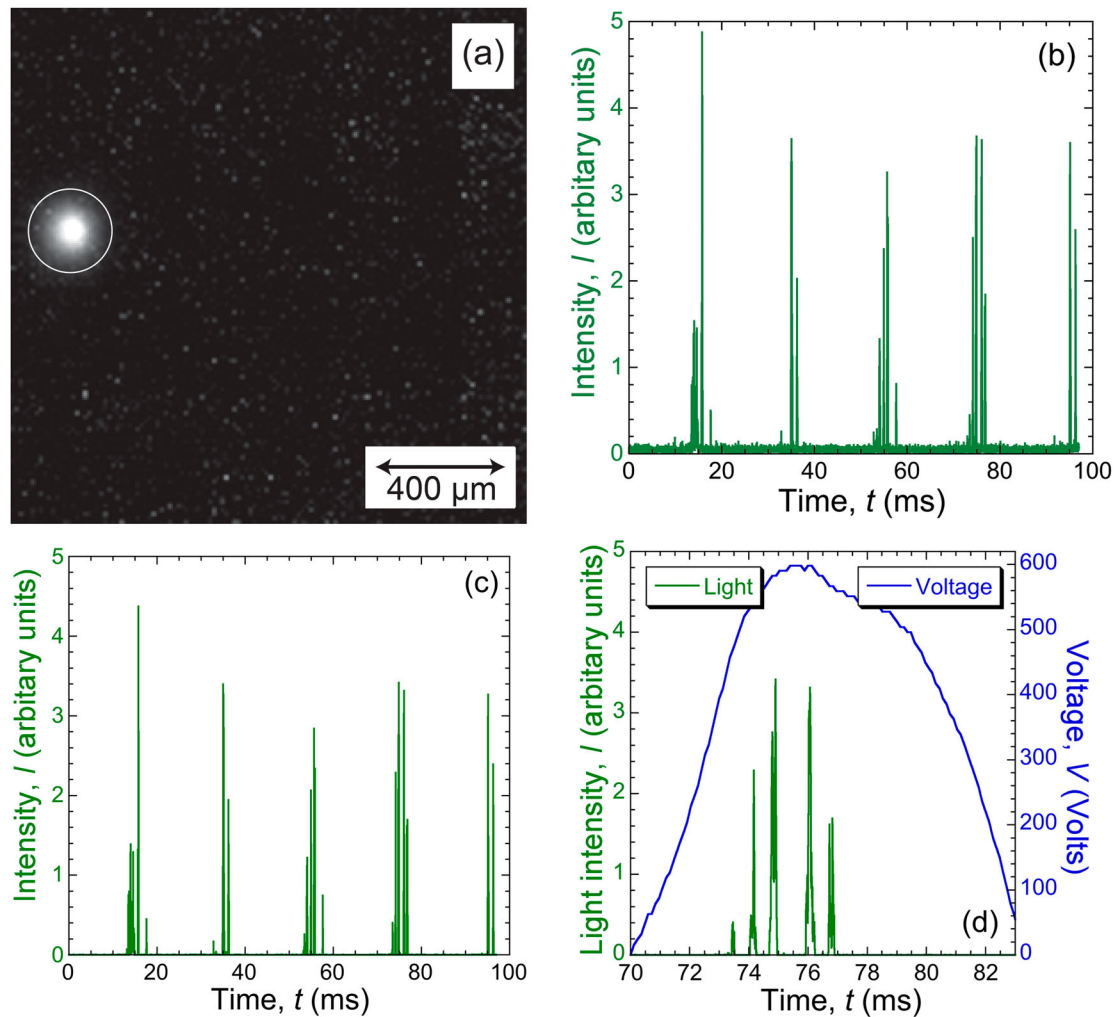
Figure 13. Information [60] from a sequence of 17,500 images (covering a period of about 0.1 s) of a region of a 50 μm thick coating on Al as PEO processing takes place, showing (a) the complete sequence superimposed, (b) total summed light intensity for each frame, as a function of time, (c) as for (b), but taken only from the bright area (circled) in (a), and (d) a higher resolution plot of part of (c), covering an anodic half-cycle, together with a typical measured voltage profile during such a period.

This is illustrated in Figure 13, which relates to a 50 μm thick coating on Al, with a sinusoidal 50 Hz supply [60]. The figure shows that, during the period concerned (∼100 ms), a series of discharges occurred at a particular location (and, at least in this case, nowhere else in the field of view, which was about 1.5 mm square). The discharges occurred only when the (anodic) applied potential was sufficiently high (>∼400 V for this case). Discharges lasted ∼100–200 μs, with incubation periods between them of ∼0.5–1 ms. These characteristics do, however, vary somewhat as the coating thickness changes, with a clear tendency for the discharges to become more energetic, and more dispersed in time and location, as the thickness increases.

Of course, a key issue concerns the relationship between discharges and the evolving microstructure of the coating, particularly the pore content and architecture. Some insights into this are provided in Figure 14, which shows SEM micrographs of a complete small area sample [62] before and after a short (∼1 s) period

of PEO processing. During this period, about 150 discharges occurred, all located at the single point where light emissions occurred – see Figure 14(b). Figures 14(c) and (d) show higher magnification views of this region. The site of the discharges (dotted red circle in Figure 14(d)) is the only location on the sample where a substantial change occurred in the appearance of the microstructure, although it can be seen that there are some very slight changes in the immediate vicinity. It was also observed [62] that, when the operation was repeated (i.e. the sample replaced in the electrolyte again, and PEO processed for a further period of ∼1 s), the cascade continued in the same location. This confirms that it must be local microstructural features that are promoting repeated discharges in the same place, rather than, for example, residual heat or some effect related to the transient distribution of electrical charge during processing. In fact, it is fairly clear that it is the presence of a deep pore that is stabilising the location of discharge sequences, creating a region of relatively low electrical resistance.
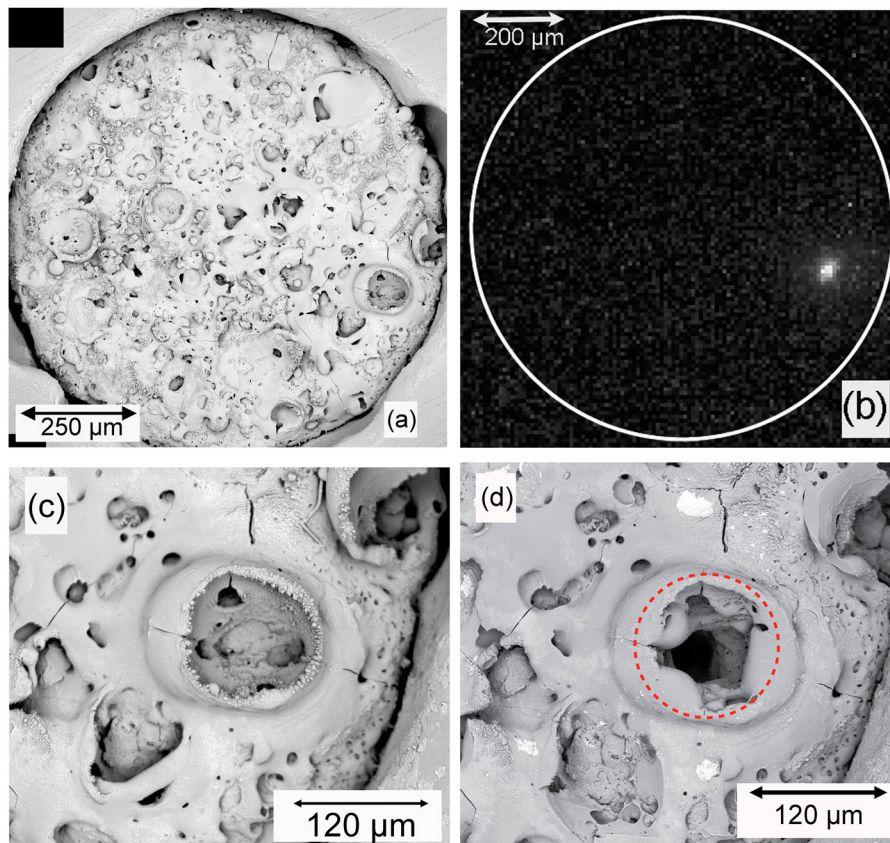
Figure 14. Microstructural effects [62] of a discharge cascade on a small area sample (with a 100 μm thick PEO coating) during processing at 2500 Hz for 1 s, showing (a) an SEM micrograph of the surface in the initial state, (b) a superimposed set of (~200,000) video images taken during the process, (c) a magnified SEM micrograph of the region indicated in (b) as the cascade location and (d) the same area after PEO processing (with the region in which the discharge was localised indicated by a circle).

Estimates [60,61] of a typical discharge energy have indicated a value of ~1 mJ and also that the conversion rate between discharge energy and resultant volume of coating is typically $\sim 10^{13}$ J m^{-3} (10^{-5} J μm^{-3}). This suggests that, for example, 1000 discharges would create $\sim 10^5$ μm^3 of oxide, corresponding to an increase in thickness of ~10 μm on a cylinder of diameter 100 μm. These are highly approximate figures, but, when the account is taken of a tendency to force liquid oxide laterally into neighbouring pores, it is plausible that a local increase in thickness of this magnitude might be sufficient to raise the electrical resistance of the locality sufficiently for the cascade concerned to terminate. (The full lifetime of an individual cascade has not yet been accurately measured, but there are indications that it might be of the order of 1000 discharges.)

3.3. Discharge lifetimes, bubble growth and incubation times

A typical architecture [62] of a pore at a cascade site is illustrated in Figure 15, which shows a top-view visualisation and a series of sections normal to the plane of the free surface for the site in Figure 14(d). These were obtained by X-ray tomography. It can be seen that the central pore extends down almost to the substrate, which is covered by just a thin layer of oxide.

This is not a very accurate way of estimating the thickness of the layer, but it can be seen that it is quite thin – of the order of a micron, or perhaps a few μm. Estimates of this order have been made by several authors [182–186]. Of course, once sufficient metal has been converted to oxide there, it will no longer be the case that the site has a lower resistance than others nearby, and the cascade will come to an end, although it is clear that this tends to happen only after a relatively large number of individual discharges have taken place.

It is also of interest to understand how a single discharge is terminated. Some insights into this can be obtained by studying the details of how the current associated with a discharge changes with time. It is important to appreciate that these characteristics are not uniform, either within a cascade or between cascades. They vary significantly with coating thickness, but also with the details of the (evolving) microstructure at the location concerned. Nevertheless, allowing for stochastic variations, some clear features can be identified. Some of these are illustrated by the plots [57] in Figure 16, which shows data obtained by statistical analysis of a large number (millions) of individual discharges, relating in this case to two different coating thicknesses. It is clear that thicker coatings lead to discharges that require a (slightly) higher initiation voltage and also have rather longer lifetimes
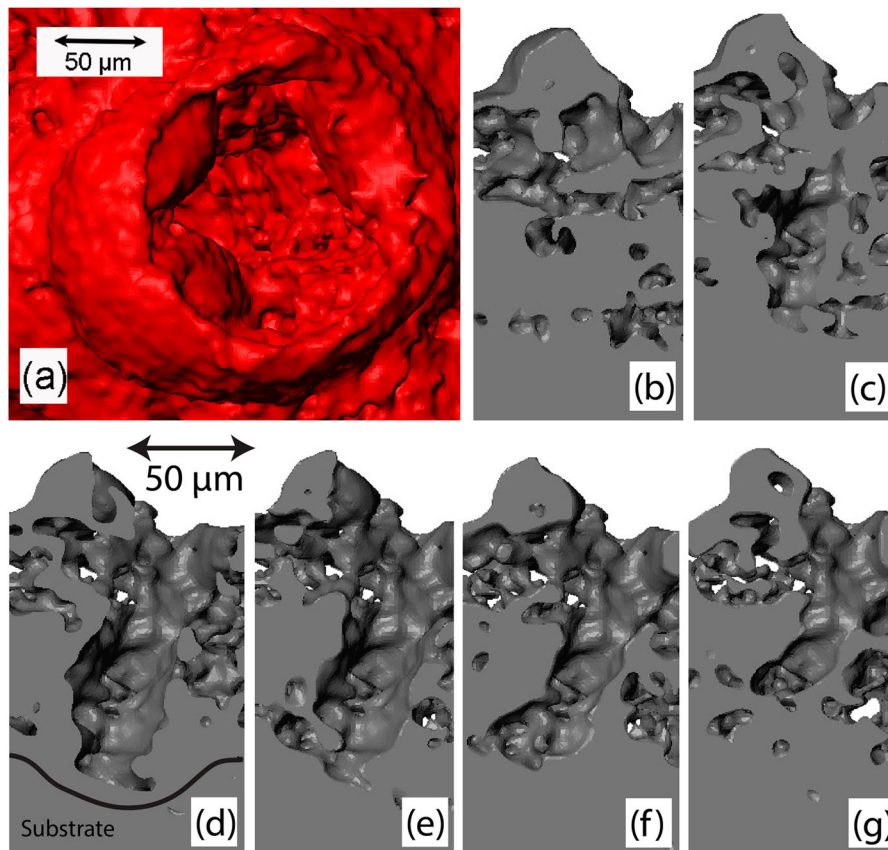
Figure 15. Tomographic data [62] from the circled region of the small area sample in Figure 10(d), showing (a) a perspective view into the pore channel and (b–g) progressive parallel sections (11 μm apart), containing the through-thickness direction, with sections (d) and (e) located near to the approximate axis of the pore.

and carry higher currents. They are clearly more energetic (but more dispersed in time and location, assuming that the overall average current and also the coating growth rate remain much the same, which is commonly the case). In fact, it is a commonplace observation that discharges tend to evolve in this way as the coating thickens.

However, there is a further point that can be noted from the shape of the plots in Figure 16, which is that the current shuts down rather abruptly, particularly with thicker coatings. There is clearly a process involved that pinches off the current flow over a short period. This implies a rapid rise in the resistance of the discharge site. This is almost certainly associated with the growth of a 'bubble' of water vapour at the top of the pore channel, where the plasma column is in contact with the bulk of the electrolyte. The discharge current is forced to flow through this expanding bubble. It will initially contain some charged species from the plasma, and will thus have a relatively high conductivity, but, as it expands due to heat flow and vaporisation of the water, these species will become dilute and the overall resistance will rise due both to an increased current flow path and to a reduced conductivity.

A number of authors [59–61,187–189] have noted that 'plasma bubbles' form at the top of discharge columns. Direct observations have been made of the growth of these bubbles, using high-intensity illumination. A sequence of video stills [61] covering the period of a single discharge lifetime (∼170 μs in this case) is shown in Figure 17. It can be seen that, as the discharge develops, a bubble rapidly grows into the water from the discharge site. It reaches a maximum diameter (of almost 1 mm in this case) in the frame having an arrow pointing to the discharge site, after which the current drops off sharply, light emission from the discharge stops and the bubble shrinks again. The rate of shrinkage is similar to the rate of growth.

A picture now emerges of the complete cycle of events during a discharge within a cascade sequence. This is illustrated in Figure 18, which shows a series of schematic sections (based on the pore architecture in one of the tomographic sections in Figure 14). The factors that control the timing of the sequence can be identified in these schematics. For example, the incubation period represents the time required for the electrolyte to flow back into the pore. It will, of course, tend to become longer as the coating thickness increases. The substrate is progressively consumed at the site of the discharge (by evaporation into the plasma) and oxide is progressively formed in the vicinity. Since the oxide normally occupies a larger volume than the
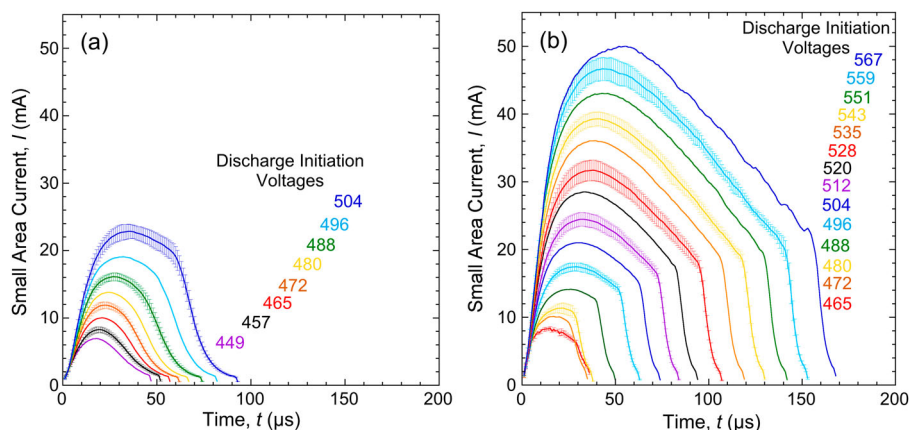
Figure 16. Plots [57] of averaged current profiles for individual discharge events, grouped according to the voltage range within which the discharge initiated, after processing periods of (a) 6 minutes and (b) 42 minutes. (The coating growth rate was about 1 μm per minute.) Error bars are shown for every other curve.

metal from which it formed (partly due to porosity in the oxide), the interface moves downward relative to the original position of the metal surface, while the free surface moves upwards. The lifetime of a cascade is presumably terminated when enough oxide has been formed in the location concerned to raise its resistance above that of alternative nearby sites. The factors controlling the lifetime of the discharge itself are a little more complex, since they involve the dynamics of plasma ignition and growth, and the rate of vaporisation of the electrolyte. Nevertheless, it may be possible to model these phenomena, and perhaps to thus gain insights into the effect of changing certain variables, such as electrolyte conductivity, coating thickness and physical properties of the oxide concerned. This is likely to be a fruitful area for future research.

3.4 PEO discharge characteristics for various metals

There is, of course, quite a lot of operational experience concerning PEO processing of different metals and it is widely recognised that the detailed outcome (microstructure, surface roughness, colour, growth rates, etc.) can depend significantly on factors such as alloy composition, electrolyte composition and electrical conditions. There are certainly variations in effects such as whether alloying elements from the substrate become incorporated in the coating (or end up in the electrolyte as the substrate is consumed), whether species from the electrolyte are deposited within the coating, etc. In this respect, the process is a particularly complex (and potentially versatile) one. Nevertheless, there are certain systematic differences between the responses of different base metals. With some, PEO
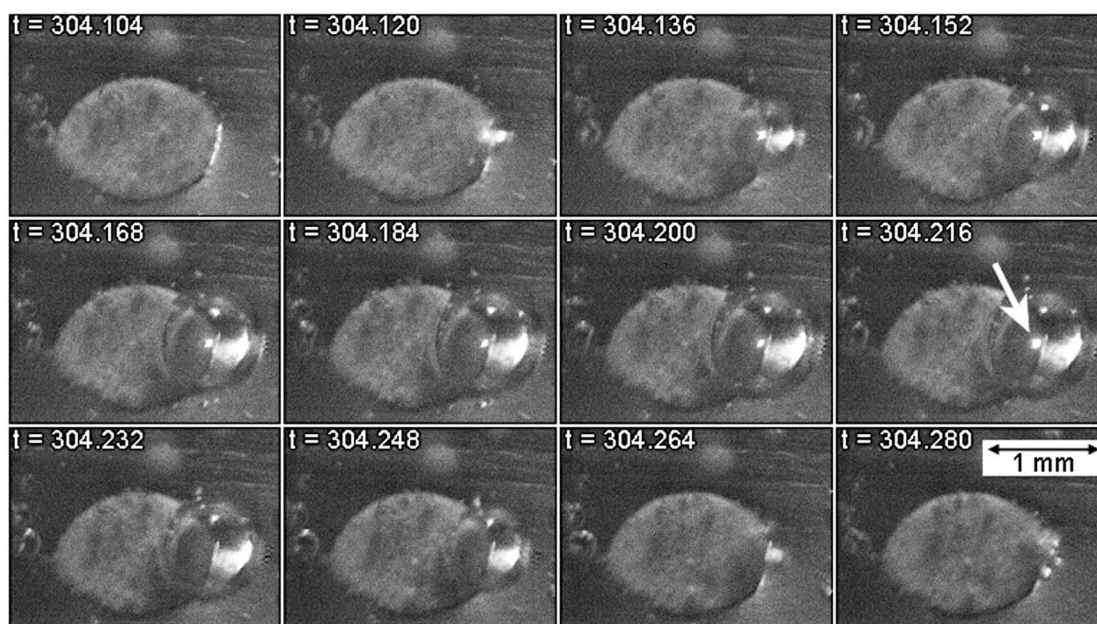

Figure 17. Sequence of video images [61] showing a small area sample (wire of diameter ~1 mm) during PEO of Al, with high-intensity external illumination. This set covers the lifetime of a single discharge event. Times are given in ms.
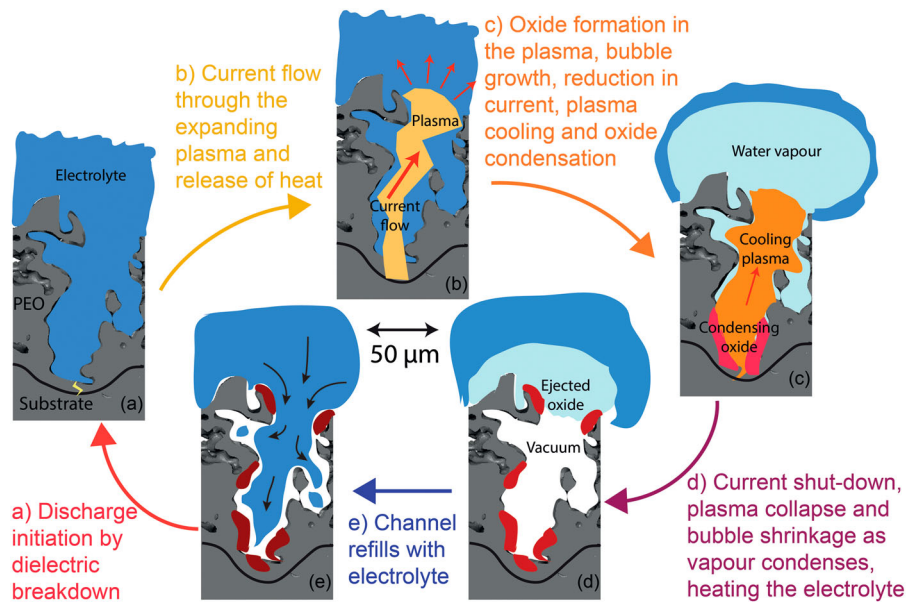
Figure 18. Sequence of schematic sections through a pore during the cycle of a single discharge event in a PEO cascade.

processing is not possible, which can largely be attributed to the thermodynamic (and related kinetic) issues outlined in Section 'Thermodynamics of oxidation during PEO'. However, there are also some clear differences between the PEO characteristics of those for which the process does 'work'.

These are illustrated by the representative voltage and (small area) current profiles shown in Figure 19 for Al, Mg, Ti and Ta. These all relate to 50 Hz processing at a point when the coating thickness was about 5–10 µm. Expanded views of the current profiles are shown in Figure 20. It is clear from Figure 4 that there is a stronger driving force for oxidation of all of these metals than there is for oxidation of hydrogen, although in the case of Ta the difference is not so large. Figure 6 shows that alumina and magnesia have large band gaps, whereas those for the oxides of Ti and Ta are significantly smaller – particularly in the case of Ti.

The plots in Figures 19 and 20 clearly show that the responses of these metals do fall into two broad categories, as might have been expected from the above points. For the Al and Mg, there were several well-defined discharges (also visible optically) during the anodic part of each cycle, when the voltage rose to 500–600 V. Current also flowed during the cathodic part, although the voltage only reached about 100 V. The other two metals, however, showed significantly different characteristics. Discharges did occur during the anodic part of the cycle, but there were more of them and their discharge currents were smaller. These current characteristics correlated with (synchronised) optical observations. Optical emissions associated with individual discharges could be detected for Ti and Ta, but they were short-lived (~10 µs) and weak. (In fact, for both Ti and Ta, it could be seen

optically that more than one discharge cascade often occurred at the same time on the small area sample: this means that the intervals between individual discharges cannot reliably be inferred from these plots, although the current associated with them should still be correct.) Also, the proportion of the total anodic current being carried by them was clearly smaller than for Al and Mg. Furthermore, the anodic voltage developed (~400 V) was somewhat lower than for Al and Mg. These observations are consistent with the idea that electron flow through the oxide layer was taking place more readily with Ti and Ta, inhibiting the development of high electric fields across the oxide and hence of large, well-defined discharges.

One or two other features of potential interest are apparent in these plots. For example, there are noticeable pulses of current in the Ti plots early in the anodic part of the cycle (and also, with lower amplitude, early in the cathodic part). These were not associated with optical emissions of any sort. This is speculative, but these current surges could be due to some kind of charge capacitive phenomenon, with the potential for complex (out of phase) effects in view of the short timescales involved. It is perhaps worth noting in this context that the dielectric constant (reflecting the capacity to store charge) of TiO_2 is much higher than that of most other oxides – see Section 'Dielectric strengths and dielectric constants of oxides'. None of the other metals exhibited any similar charge pulsing, although there were some (small) discharges in the cathodic part of the cycle with Ta.

More generally, it may be noted that there is clearly scope for complex charge redistribution effects to arise during PEO, both in the coating material itself and in the electrolyte within and adjacent to the coating. Several recent publications have emphasised the
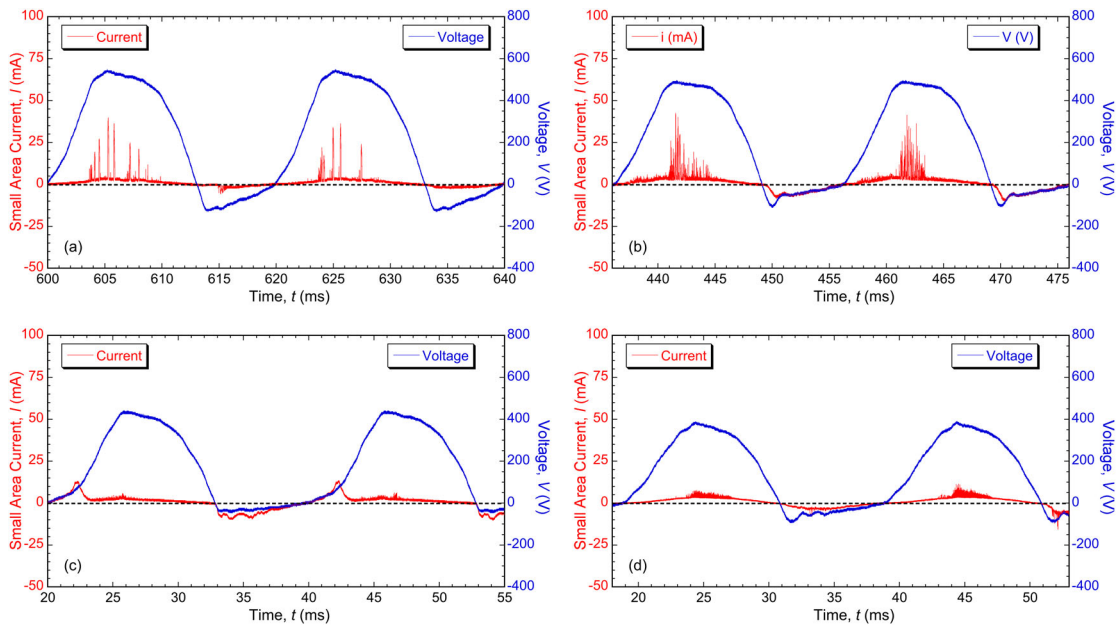
Figure 19. Voltage and (small area) current profiles for 50 Hz processing of (a) Al, (b) Mg, (c) Ti and (d) Ta.

potentially important role of charge accumulation, particularly at the interface between coating and electrolyte. For example, Martin et al. [65] reported that formation of discharges may be delayed by this accumulation, making them less energetic (and thus potentially less likely to cause damage to the existing coating).

3.5 Gas evolution

PEO is normally carried out using an AC supply, with the electrical circuitry often set such that the current (i.e. the current density) is fixed and is the same in both anodic and cathodic parts of the cycle. For metals that are well suited to PEO processing, at least most of

the current flowing in the anodic part of the cycle is carried in the form of discharges (that stimulate oxidation of the substrate). These discharges are initiated by the flow of electrons from the electrolyte to the substrate, through the residual oxide layer, in some kind of avalanche process that leads to plasma formation and growth. Hydroxyl anions could lose electrons to form oxygen gas (as in conventional electrolysis of water), but during (successful) PEO this process is likely to be interrupted by the plasma formation. It seems likely that these ions, and possibly oxygen molecules that have just been formed, will become incorporated into the plasma. Of course, they will not be the only source of oxygen in the plasma, since water molecules will also enter it (and become ionised). Some of this oxygen is
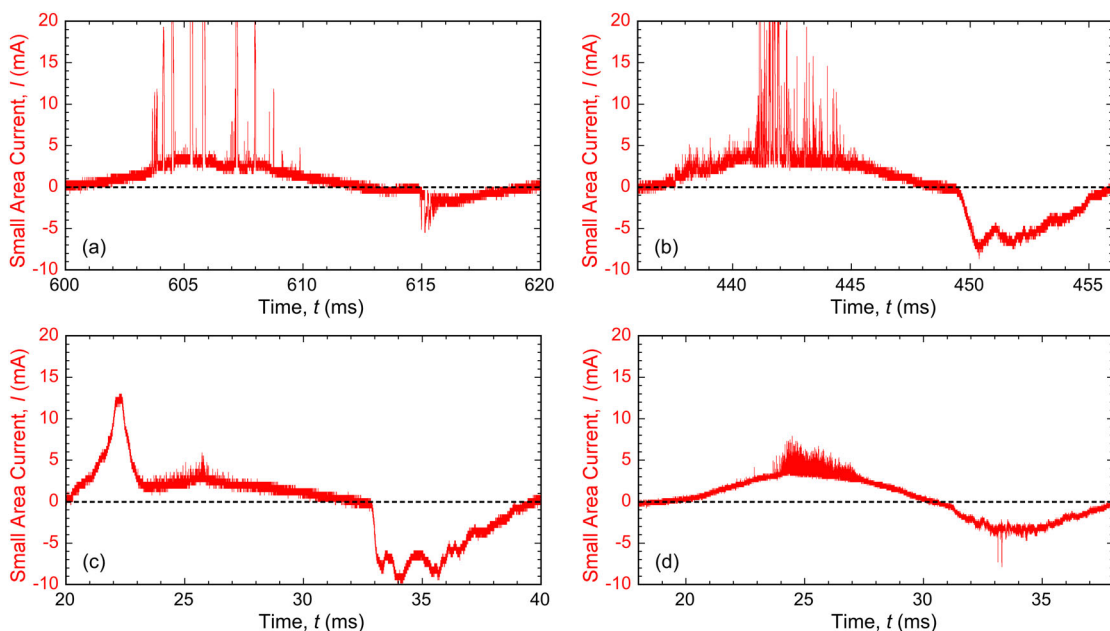

Figure 20. Expanded current profile plots for the data in Figure 19.

then likely to combine with metal cations in the plasma as it cools down during its collapse, particularly if the thermodynamic driving force for this is greater than for the (re)formation of water.

In general, it is thus expected that, if PEO is proceeding successfully, with most of the current flowing via plasma discharges, then there should on this basis be little or no evolution of oxygen gas during the anodic half-cycle. It is perhaps worth mentioning in this context that there has been a relatively little direct experimental investigation of the rates or types of gas evolution during PEO. Nevertheless, there has been some systematic work and a consistent finding [190–192] is gas evolution rates considerably above the Faraday yield level (corresponding to conventional electrolysis of water). Figure 21 shows an example plot [192] of the voltage and the quantity of gas evolved (at the anode) during a typical PEO run, with it being reported in this case that virtually all of the gas was oxygen (although other reports suggest that hydrogen can also be formed at the anode). It can be seen that, once PEO discharges had become established (at ~500 V), gas evolution started and the rate of gas production remained approximately constant (~0.6 L m^{-2} s^{-1}) after this. Since the current density was 935 A m^{-2}, the maximum rate of gas evolution during conventional electrolysis (Faraday yield) would have been $935 \times 22.4/(4 \times 96,485)$ ~ 0.05 L m^{-2} s^{-1}, so the observed rate is an order of magnitude greater than the maximum expected value. Of course, it is clear that PEO is not a conventional electro-chemical process, but the source of this gas is nevertheless of interest.

In fact, it seems clear that this gas must come from the plasma. Various species enter the plasma, but, in terms of quantity, a lot of these are produced by breakdown of water. It is clear from Section 'Discharge lifetimes, bubble growth and incubation times' that the quantity of gas produced during each discharge is far greater than that needed to account for the net rate of gas evolution evident in Figure 21. Of course, most of the hydrogen and oxygen in the plasma will recombine as it cools to recreate the water. However, the quenching is very rapid and it is certainly plausible that some residual gas could be left, perhaps partly because an imbalance between hydrogen and oxygen had been created as the plasma cooled. Of course, this mechanism, which is not electro-chemical in nature, would not be subject to Faraday yield limits – the quantity of gas potentially available would only be limited by the total energy input, which is normally substantial.

Such effects, which could take place within both anodic and cathodic plasmas, are likely to confuse the interpretation of gas evolution rates. However, it does in any event seem clear that, in the cathodic part of the cycle, there is a high likelihood of hydrogen ions being able to move rapidly through the electrolyte to the surface of the residual oxide layer, and there acquire electrons that have passed through the layer, so that hydrogen gas is evolved. This may depend on how effectively the surface concerned catalyses this hydrogen ion discharge – as indeed it does during conventional electrolysis of water [193]– but it is certainly well known in practical terms that hydrogen gas does tend to be evolved at relatively high rates during PEO. The notion of the 'valve metals' presumably arose from the idea that electrons could move through the oxide layer in this direction (without causing dielectric breakdown), but not in the other direction (from electrolyte to metal). However, as outlined in Section 'The "valve metals" and charge transfer during anodising and PEO', there is no clear reason to expect this. An alternative explanation is that the high mobility of H$^+$ ions in the electrolyte allows them to reach the oxide surface at rates sufficient to carry much of the imposed current, reducing the field across the oxide layer and hence the likelihood of dielectric breakdown. If this is indeed largely a dynamic effect, then some dependence on supply frequency might be expected. This is explored in the next section.

3.6. Cathodic discharges and the effect of supply frequency

The cathodic part of the cycle has been increasingly studied recently. It has been clear for some time [194] that PEO coatings produced using AC are in general of superior quality (harder and denser, for example) than those produced under corresponding (anodic) DC conditions. It has also been shown that coating quality is improved if the cathodic voltage is raised [90] or if the ratio of cathodic current to anodic current is increased [195]. What actually happens during the cathodic half-cycle is less clear. It is certainly the case that, at least under most conditions, discharges predominantly occur during the anodic half-cycle, although current does flow in both half-cycles.

However, discharges have been observed in the cathodic half-cycle under some conditions, particularly when the electrolyte is strongly alkaline [172,196–198] and for relatively thick coatings. It is also worth noting that PEO coatings have been produced under conditions in which cathodic discharges predominate. For example, Stojadinovic et al. [54] reported cathodic PEO of Mo. It certainly seems likely that substrate material can become oxidised as readily within a cathodic discharge as within an anodic one. On the other hand, while there have been suggestions about this [199,200], the mechanism of charge transfer during the cathodic part of the cycle, in the absence of cathodic discharges, is often rather unclear. A likely one, however, is simply the discharge of hydrogen ions (protons), leading to evolution of hydrogen gas – see
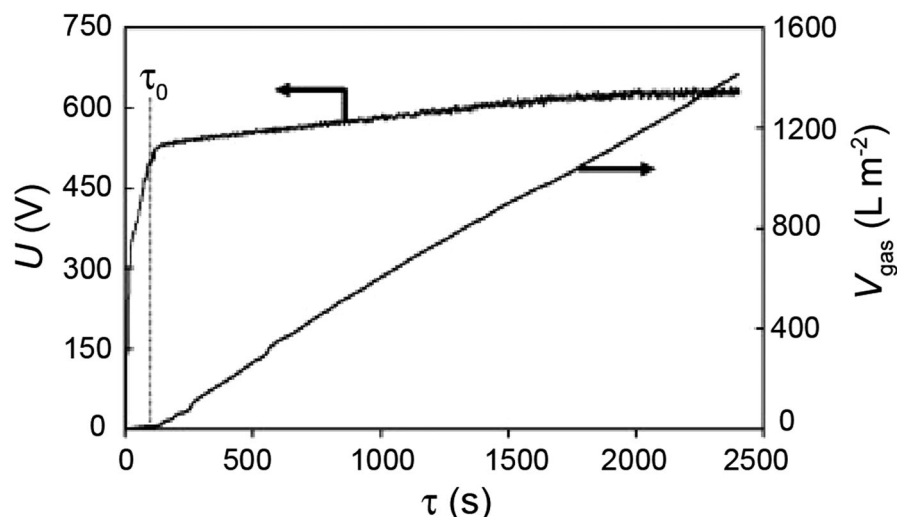
Figure 21. Experimental data [192] for gas evolution and voltage development during PEO of 6082 Al, with an electrolyte containing 1 g L^{-1} of KOH and a current density of 935 A m^{-2}.

Section 'Gas evolution'. Of course, this is unproductive in terms of coating growth, although it is possible that the associated charge redistribution could help promote the anodic discharges in some way. The fact that cathodic discharges appear to be favoured by strongly alkaline electrolytes (and by the coating already being relatively thick) may relate to inhibition of hydrogen gas formation (respectively via a shortage of protons and a greater difficulty in moving them through the coating).

In practice, PEO processing is conventionally carried out using AC, with most coatings, both in research work and in technological usage, often being produced at 50 or 60 Hz (although higher frequencies are becoming more popular). The cycle period is thus commonly about 20 ms, which is sufficiently long to allow extended cascades during each (anodic) half-cycle. There is considerable interest in how the process changes as the supply frequency is increased, such that the cycle period is no longer large compared with the inter-discharge period, or the discharge period itself. There are several reports [22,201,202] that an increase in the supply frequency (with maximum values usually around 1.0–1.5 kHz) leads to a reduction in coating growth rates, although it must be recognised that others have reported different effects [24,203,204] and, as with many aspects of PEO, there is considerable complexity and scope for extraneous factors to exert an influence. There have also been reports that the coating microstructure becomes finer and denser as the frequency is increased, which might be regarded as beneficial.

It is clearly of interest to examine the effect of frequency on the (small area) current . Figure 22(a) shows a typical (square wave) voltage profile during a single 50 Hz cycle (i.e. over a period of 20 ms), at a stage when the coating thickness was about 50 μm. It can be seen that the anodic voltage was ~600 V, while the cathodic voltage was ~125 V. Figure 22(b) shows corresponding currents, both the total and that through the small area sample. Apart from short initial transients, the total current was just above 2 A throughout both anodic and cathodic half-cycles (corresponding to the pre-selected current density). The cathodic current through the small area is consistent with the total current (taking account of the area ratio between small and large samples, and also the greater significance of edge effects for the small sample). This suggests a cathodic process that is smooth and continuous, such as might be expected for conversion of protons to hydrogen gas. In contrast to this, the anodic current is made up of a series of current pulses corresponding to discharges.

As the supply frequency was increased, and the half-cycle period started to approach typical lifetimes of the discharges, changes were observed in the nature of the voltage and current profiles (although, as with the 50 Hz case, there were some cycles in which no discharges occurred on the small sample). Figure 22 (c) and (d), which show profiles from experiments carried out at 2.5 kHz, illustrates these changes. The half-cycle period is now 200 μs, similar to a typical discharge lifetime. The voltage profiles (Figure 22 (c)) are similar to those at 50 Hz (Figure 17(a)), except that the cathodic voltage has risen to about 250 V, compared to 125 V at 50 Hz, while the anodic voltage remained unchanged at about 600 V. This suggests a switch to a cathodic process that requires a larger driving force. It is also clear from the current profiles (Figure 22(d)) for the small area that changes have occurred in phenomena occurring during the cathodic part of the cycle. While the anodic discharges are still taking place (with approximately unchanged lifetimes, of the order of 100–200 μs – now occupying
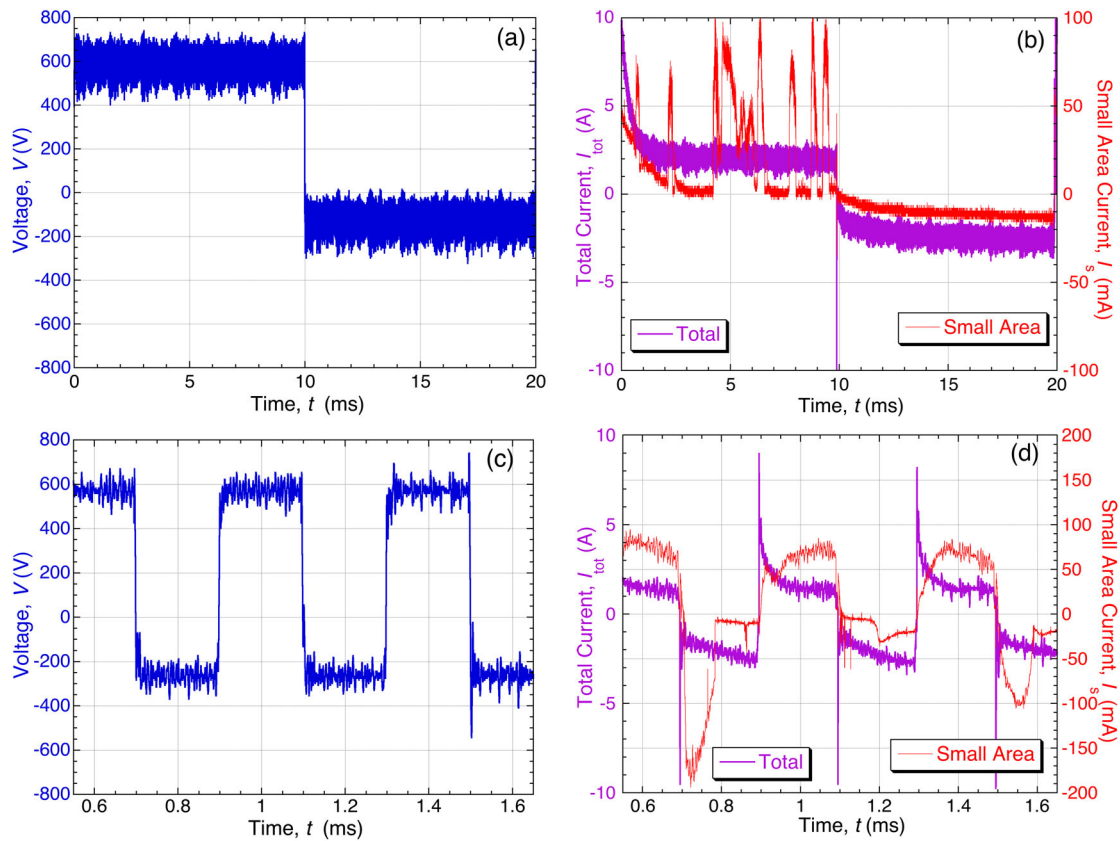
Figure 22. Synchronised profiles of voltage and current (bulk and small area) during PEO of an Al alloy, for supply frequencies of 50 Hz (a and b) and 2500 Hz (c and d).

most of the half-cycle – and also similar current levels of ~50–100 mA), there are now clear current pulses in the cathodic part of the cycle as well. Moreover, some of these pulses rise to higher current levels than those of the anodic discharges, with peaks approaching 200 mA. Their lifetimes are similar to the anodic pulses, although with an apparent tendency to be slightly shorter (<~100 μs).

Confirmation that these cathodic pulses correspond to discharges is provided by high-speed photography observations, with the images in Figure 23 showing that light emission accompanies both anodic and cathodic pulses. It also appears that, as for the anodic discharges, those in the cathodic half-cycle also occur in spatially localised 'cascades', although the two types of discharge occur in different locations. This is unsurprising, since the periods between discharges in a cascade are thought to be required for re-filling of the pore by electrolyte, so that the site would not be available for a cascade of the opposite 'sign' (during high frequency operation).

There may be potential for increased energy efficiency by promoting discharges in the cathodic part of the cycle, since it seems likely that these will lead to coating growth, whereas hydrogen evolution will not do this (and is also potentially hazardous). The issue of energy efficiency is addressed in Section 'Energy consumption'.

3.7. 'Soft Plasma' PEO conditions

Over recent years, increasing attention has been paid to the so-called soft-sparking or soft' regime during PEO [24,63,184,200,205–212]. Normally, as the thickness of a PEO coating increases, the through-thickness electrical discharges become more intense and longer-lived. This often places an upper limit on the thickness of PEO coatings, since intense discharges start to destroy the coating. However, under certain conditions, termed the soft regime, it appears that this can be avoided and coating microstructures can be improved.

In such cases, the process starts conventionally, but, once a certain coating thickness or processing time has been reached, a reduction is observed in the applied potential (under constant current conditions [63]– see Figure 24) and the discharges become almost invisible (although coating growth continues). This is illustrated [205] in Figure 25 – note that (d) has an integration time longer than (a)–(c) by a factor of 200: clearly, the quantity of light being emitted is much less in this case, although it can be seen in Figure 25(d) that there still appear to be preferred locations for its emission. This 'soft' regime was first studied by Jaspard-Mécuson et al. [205], who asserted that the ratio of anodic to cathodic charge (termed the charge ratio, R) must be less than unity for the transition to occur. This does appear to be an important
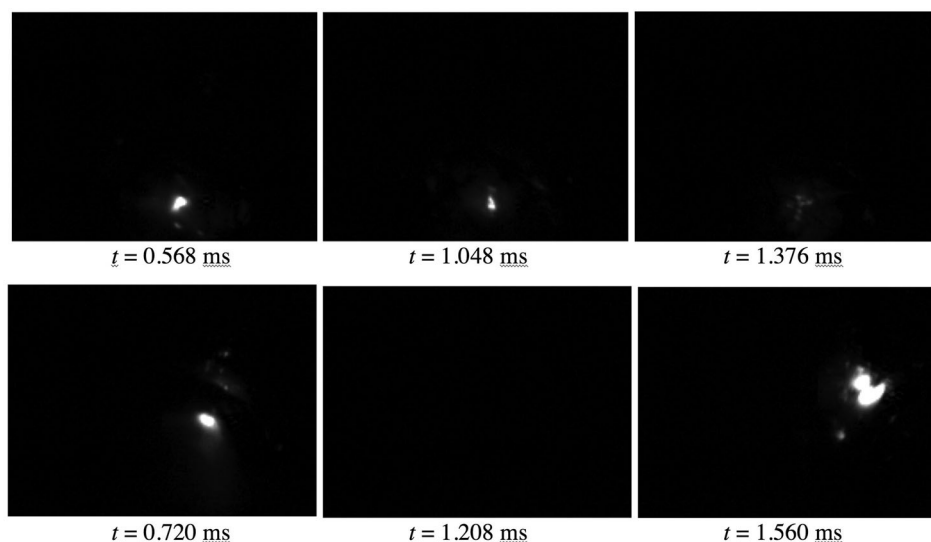
Figure 23. Set of stills from a high-speed video taken during PEO processing at 2.5 kHz, with the times corresponding to those in Figure 22(c) and (d).
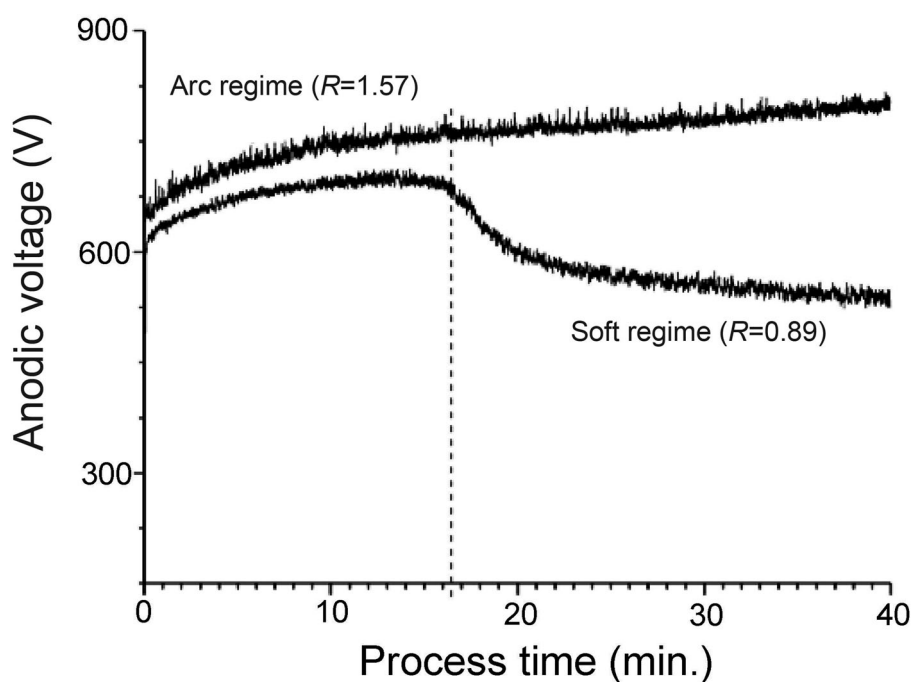

Figure 24. Evolution of the anodic voltage over the process duration under standard conditions (termed arc regime) and soft regime conditions, with the transition to soft regime indicated by the dashed line [63].

factor, since virtually all subsequent studies concerning the soft regime report using larger cathodic than anodic rates of charge transfer, although it remains unclear why this is needed. Additionally, the transition to the soft regime apparently occurs sooner for higher current densities and higher AC supply frequencies [24], and also as the electrolyte gets older [39]. The literature is largely focused on Al, but there are also reports for Mg [184], Zr [89,213] and pre-anodised Al [207,208]. The concept of a pre-anodised layer on Al is of interest, since as it apparently accelerates the transition. This may constitute evidence that coating thickness plays an important role in the transition. It has also been

suggested that this pre-anodising step apparently reduces the overall energy consumption.

Polished cross-sections of these coatings do not appear to exhibit large through-thickness pore channels, although examination of these microstructures on such sections can be misleading, due to the effects of the polishing. More convincing is the observation that the diameters of 'melt-pools' formed around discharge channels remain approximately constant [205] after the soft regime has been established (whereas, under standard conditions, these diameters tend to increase linearly with processing time). In a tracer study [209], it was found that all new coating growth
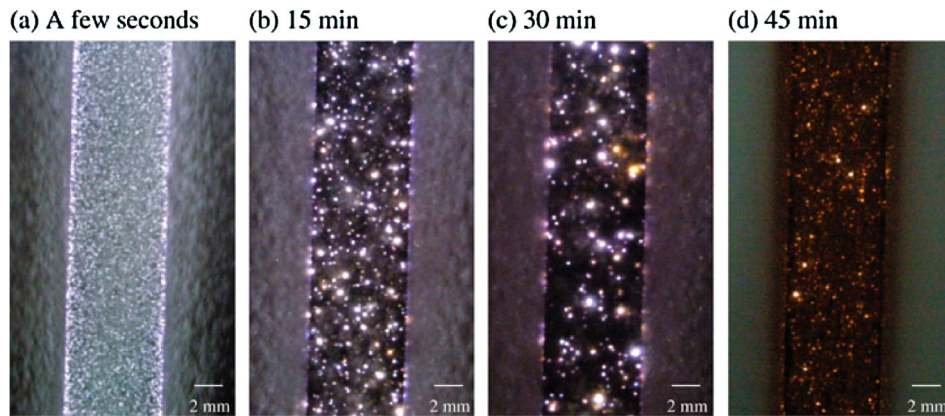
Figure 25. Side-view photos [205] of aluminium alloy samples at a different time during PEO processing ($R = 0.89$). The integration time was between 8 and 10 ms for photos (a–c), but 2000 ms for photo (d).

occurred at the substrate-coating interface after the transition to lower applied potential occurred, which would explain why the melt-pool diameters on the coating-free surface remain constant. The reduction in the applied potential during the transition to the soft regime suggests that the power consumed during processing in the soft regime should fall. Interestingly, the growth rate of the coating actually appears to increase after the transition [205], although there is no doubt that more work is needed to confirm such effects, partly because the techniques used to measure coating thickness are often rather inaccurate.

Clearly, this transition could be of considerable industrial interest, since one of the major issues with PEO is its relatively high energy consumption – see Section 'Energy consumption'. In fact, data have been published that give information about such a reduction in rates of energy consumption as the soft regime is entered. Figure 26 shows how the reduction in anodic potential that accompanies the onset of the soft regime occurs earlier when R is lower, and also plots the associated reduction in specific energy consumption rate [210]. It can be seen that there is a significant fall (of around 40%). None of these publications, however, has presented a mechanistic explanation of how or why the process is taking place differently in the soft regime. Furthermore, it does need to be convincingly confirmed that the rate of coating growth does not fall as the soft regime becomes established.

A possible explanation for the soft regime is that a large number of small discharges are taking place at the metal/oxide interface, but these are not developing in the way that they normally do, and so do not reach the free surface of the coating (such that there is little or no light emission). This is, however, not entirely consistent with information such as that in Figure 25(d) and it is clear that further study is needed. At present, it is unclear whether such (small) individual discharges can be identified in some way (e.g. using the small area monitoring technique) or even whether they are anodic and/or cathodic. Also, there is no explanation so far of

why raising the potential (or the charge flow) in the cathodic part of the cycle should stimulate this transition, or any indication of the effects of changing the electrolyte composition (e.g. the pH). It may also be noted that suggestions have been made [200] to the effect that the soft regime may represent a reversion to the growth mechanisms that predominate during anodisation. In summary, however, it cannot at present be said that the 'soft regime' is well characterised. Reliable guidelines for ensuring that operation takes place in this regime are not yet available and the potential benefits have not been confirmed or systematically exploited. It seems unlikely that this will be possible until it is much better understood.

3.8. Energy consumption

While these figures are necessarily very approximate, it has been estimated [60,61] that a typical discharge energy is ∼1 mJ and that the conversion rate between discharge energy and resultant volume of coating is typically ∼10^{13} J m^{-3} (10^{-5} J μm^{-3}). This can also be expressed as about 3 kWh μm^{-1} m^{-2}, which are the units used, for example, in Figure 26. It follows that, during a 1 s PEO treatment, with ∼300 localised discharges occurring on the small area sample, about 0.3 J of energy was absorbed there, creating about 3×10^4 μm^3 of oxide (cube of side ∼30 μm, or, on a cylinder of diameter 100 μm, an increase in length of about 4 μm). Of course, much of this oxide was probably created near the interface with the substrate and a relatively small proportion ejected through the discharge channel onto the free surface. It is also likely that molten oxide gets injected under the pressure of the discharge into neighbouring interconnected pores.

A study has been undertaken of the energies absorbed by various phenomena taking place during PEO – melting and vaporisation of substrate, melting of existing oxide coating, initiation and sustaining of the plasma, vaporisation of water, electrical heating
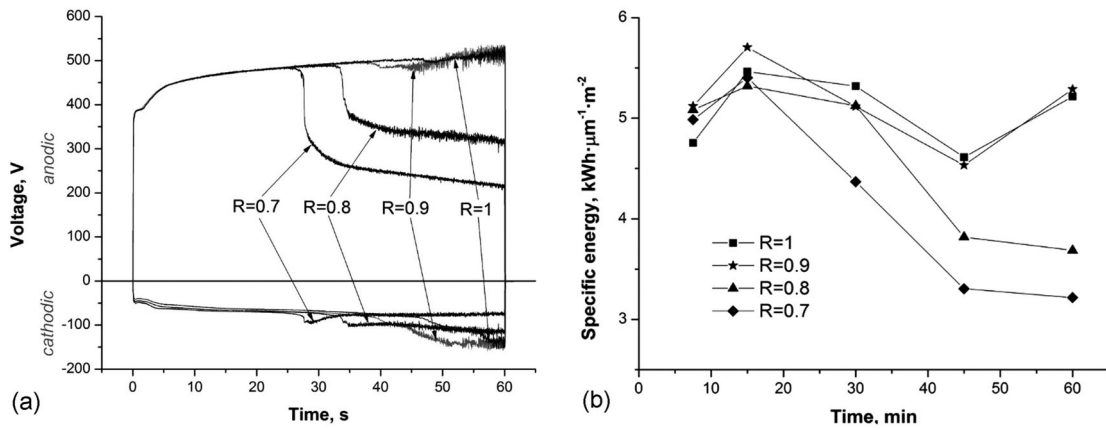
Figure 26. Plots of data [210] obtained during PEO processing of Al at 50 Hz, with a fixed anodic current density of 10 A dm^{-2} and four different values of R (ratio of anodic to cathodic current densities), showing (a) anodic and cathodic voltages needed to maintain these current densities and (b) corresponding rates of energy consumption, per unit volume of coating produced.
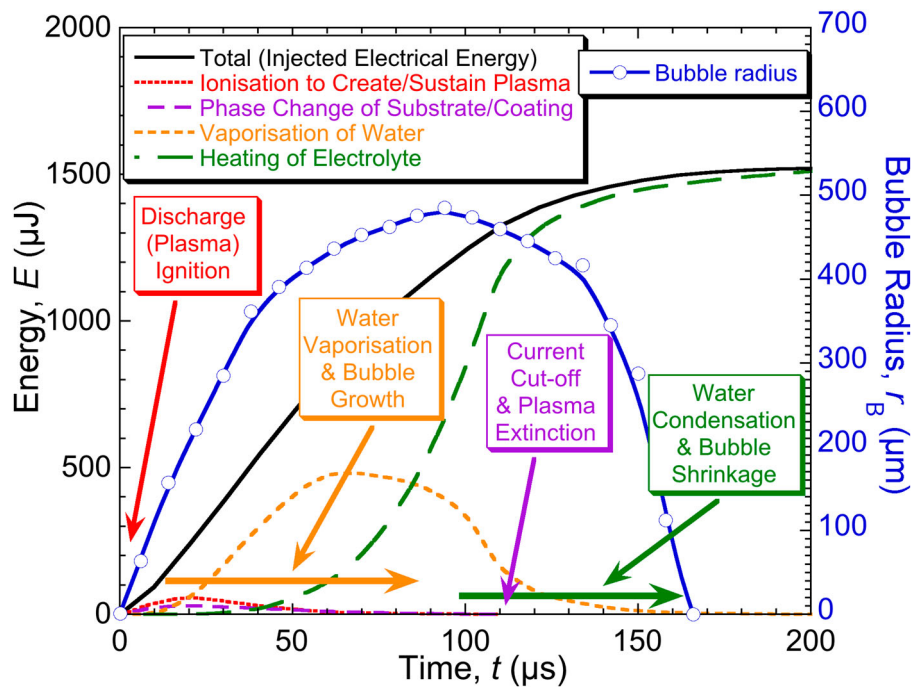

Figure 27. Semi-quantitative plot [61] showing how the total (electrically injected) energy changes during the formation of an individual discharge, and how it is converted between different forms during and immediately after the discharge period.

of the electrolyte and conversion of metal to oxide (which releases energy, rather than absorbing it). A semi-quantitative graphical presentation of the energetics involved [61] is shown in Figure 27. It can be seen that most of the injected energy is (transiently) absorbed in the form of vaporisation of water, after which it will inevitably end up as rather low-grade (difficult to recover) energy in the form of a large mass of (moderately) heated electrolyte. The energy released by oxidation of the metal is not included in the plot, since its magnitude is small compared with these absorbed energies.

There does not appear to be any immediately obvious way of reducing this energy wastage, although improved understanding of details such as those

presented here is certainly of potential value in considering various measures. The basic problem appears to be that exposing the substrate to oxidising agents via these highly energetic discharges is very inefficient, at least under the conditions conventionally employed. There have been studies [66,214,215] aimed specifically at energy efficiency, and one or two suggestions made about measures, such as the use of a grid cathode [216], that could be helpful. The most promising approach is probably to somehow reduce the energy associated with each discharge (while retaining a similar rate of transformation of substrate), possibly by reducing the voltage needed for it to occur, or to promote more transformation per discharge (while retaining a similar discharge energy). Further study of the details of the

energetics of the process is clearly likely to be helpful in pursuing such aims.

4. Summary and prospects

The PEO process has constituted a recognised coating technology for well over 30 years and has been in significant commercial use for most of that time. It has a number of characteristics that make it almost unique, and potentially very attractive. One of these is that the process involves a continuous restructuring of the coating throughout its thickness, tending to reduce residual stress levels and improve its through-thickness homogeneity. Another is that, since coatings are created via partial consumption of the substrate, they tend to exhibit excellent interfacial adhesion. On the other hand, the resultant coatings are certainly not free from what might be regarded as defects – indeed, they tend to contain a lot of porosity, microcracks, inclusions, etc. These arise from the inherent nature of the process, which involves the repeated formation of plasma discharges through the thickness of the existing coating, with new coating material being created as they collapse, after which it is rapidly injected into surrounding regions. These events are highly transient and create rapid cooling and high thermal gradients, so it is unsurprising that the coating microstructure should be disordered and metastable. However, the effects of these microstructural features are largely beneficial. The porosity confers a low stiffness and hence a high strain tolerance, which (in combination with the good interfacial adhesion) leads to excellent spallation resistance. Moreover, while they tend to be porous and compliant, PEO coatings often have a high hardness and exhibit good wear resistance. They are also excellent keying surfaces for further treatment, such as painting and adhesive bonding, or for particular types of functionality, such as catalytic or biomedical activity.

It is also important to recognise that the PEO process is a very versatile one. There are many process variables, most of them associated with the composition of the electrolyte and the parameters of the electrical supply. These variables can have profound effects on the coating microstructure, hence influencing important characteristics such as colour, texture, hardness, permeability and specific surface area. There is therefore enormous scope for tailoring PEO coatings to their planned functionality. There are, however, certain challenges involved in expanding their usage to fulfil such promise. A key one, central to the objectives of this review, is to obtain an improved understanding of the process–microstructure–property relationships, which are probably less well understood in the PEO area than in virtually any other type of processing technology in commercial use. The main hurdle here concerns the pivotal role of the individual discharges, which are highly complex, short-lived events. Background knowledge from various fields (plasma physics, electro-chemistry, electrical engineering, transport phenomena, heat transfer, etc.) is required in order to obtain a full picture of their influence on process characteristics and on coating structure and properties. There is no doubt that, while progress is being made, the current picture is in fact far from complete. Nevertheless, the transition from a purely empirical selection of conditions for particular requirements to an entirely logical design procedure is well under way. This should in due course allow various types of systematic optimisation, reduction of energy consumption, tailoring of coating properties, etc., leading to considerably expanded usage.

Disclosure statement

No potential conflict of interest was reported by the authors.

ORCID

Trevor William Clyne http://orcid.org/0000-0003-2163-1840
Samuel Christopher Troughton http://orcid.org/0000-0003-2413-5455

References

[1] Skeldon P, Thompson GE, Wood GC. Formation of relatively pure alumina films by anodic polarization. *Thin Solid Films*. 1987;148:333–341.
[2] Mota RO, Liu Y, Mattos OR, et al. Influences of ion migration and electric field on the layered anodic films on Al-Mg alloys. *Corros Sci*. 2008;50:1391–1396.
[3] Li FY, Zhang L, Metzger RM. On the growth of highly ordered pores in anodized aluminum oxide. *Chem Mater*. 1998;10:2470–2480.

[4] Macak JM, Tsuchiya H, Schmuki P. High-aspect-ratio TiO2 nanotubes by anodization of titanium. *Angew Chem Int Edn*. 2005;44:2100–2102.

[5] Blawert C, Dietzel W, Ghali E, et al. Anodizing treatments for magnesium alloys and their effect on corrosion resistance in various environments. *Adv Eng Mater*. 2006;8:511–533.

[6] Wong YH, Affendy MG, Lau SK, et al. Effects of anodisation parameters on thin film properties: a review. *Mat Sci Technol*. 2017;33:699–711.

[7] Lee W, Ji R, Gosele U, et al. Fast fabrication of long-range ordered porous alumina membranes by hard anodization. *Nat Mater*. 2006;5:741–747.

[8] Bozza A, Giovanardi R, Manfredini T, et al. Pulsed current effect on hard anodizing process of 7075-T6 aluminium alloy. *Surf Coat Technol*. 2015;270:139–144.

[9] Cheng Y, Matykina E, Skeldon P, et al. Characterization of plasma electrolytic oxidation coatings on zircaloy-4 formed in different electrolytes with AC current regime. *Electrochim Acta*. 2011;56:8467–8476.

[10] Cheng Y, Matykina E, Arrabal R, et al. Plasma electrolytic oxidation and corrosion protection of zircaloy-4. *Surf Coat Technol*. 2012;206:3230–3239.

[11] Lesnevskiy LN, Lyakhovetskiy MA, Ivanova SV, et al. Structure and properties of surface layers formed on zirconium alloy by microarc oxidation. *J Surf Invest*. 2016;10:641–647.

[12] Duan ZG, Yang HL, Satoh Y, et al. Current status of materials development of nuclear fuel cladding tubes for light water reactors. *Nucl Eng Des*. 2017;316:131–150.

[13] Wang P, Li JP, Guo YC, et al. Ceramic coating formation on high Si containing Al alloy by PEO process. *Surf Eng*. 2016;32:428–434.

[14] He J, Cai QZ, Luo HH, et al. Influence of silicon on growth process of plasma electrolytic oxidation coating on Al-Si alloy. *J Alloys Compd*. 2009;471:395–399.

[15] Kim YM, Hwang DY, Lee CW, et al. Surface modification of high Si content Al alloy by plasma electrolytic oxidation. *Korean J Met Mat*. 2010;48:49–56.

[16] Xu F, Xia Y, Li G. The mechanism of PEO process on Al-Si alloys with the bulk primary silicon. *Appl Surf Sci*. 2009;255:9531–9538.

[17] Arrabal R, Matykina E, Skeldon P, et al. Coating formation by plasma electrolytic oxidation on ZC71/SiC/12p-T6 magnesium metal matrix composite. *Appl Surf Sci*. 2009;255:5071–5078.

[18] Cui SH, Han JM, Du YP, et al. Corrosion resistance and wear resistance of plasma electrolytic oxidation coatings on metal matrix composites. *Surf Coat Technol*. 2007;201:5306–5309.

[19] Gu WC, Shen DJ, Wang YL, et al. Deposition of duplex Al_2O_3/aluminum coatings on steel using a combined technique of arc spraying and plasma electrolytic oxidation. *Appl Surf Sci*. 2006;252:2927–2932.

[20] Gu W, Lv G, Chen H, et al. Preparation of ceramic coatings on inner surface of steel tubes using a combined technique of hot-dipping and plasma electrolytic oxidation. *J Alloys Compd*. 2007;430:308–312.

[21] Zhao JH, Zhao GH, Li T, et al. Structure and properties of composite ceramic coatings on H13 steel by hot dipping aluminum and plasma electrolytic oxidation. *Cailiao Rechuli Xuebao/Trans Mater Heat Treat*. 2012;33:129–132.

[22] Kharanagh VJ, Sani MAF, Rafizadeh E. Effect of current frequency on coating properties formed on aluminised steel by plasma electrolytic oxidation. *Surf Eng*. 2014;30:224–228.

[23] Yang W, Yang SY, Zhao YF, et al. *High power current pulse power supply for micro-arc oxidation*. New York: IEEE; 2009.

[24] Martin J, Melhem A, Shchedrina I, et al. Effects of electrical parameters on plasma electrolytic oxidation of aluminium. *Surf Coat Technol*. 2013;221:70–76.

[25] Yao ZP, Wang DL, Xia QX, et al. Effect of PEO power modes on structure and corrosion resistance of ceramic coatings on AZ91D Mg alloy. *Surf Eng*. 2012;28:96–101.

[26] Tran QP, Kuo YC, Sun JK, et al. High quality oxide-layers on Al-alloy by micro-arc oxidation using hybrid voltages. *Surf Coat Technol*. 2016;303:61–67.

[27] Stojadinovic S, Vasilic R, Petkovic M, et al. Luminescence properties of oxide films formed by anodization of aluminum in 12-tungstophosphoric acid. *Electrochim Acta*. 2010;55:3857–3863.

[28] Stojadinović S, Vasilić R, Petković M, et al. Plasma electrolytic oxidation of titanium in heteropolytungstate acids. *Surf Coat Technol*. 2011;206:575–581.

[29] Petković M, Stojadinović S, Vasilić R, et al. Characterization of oxide coatings formed on tantalum by plasma electrolytic oxidation in 12-tungstosilicic acid. *Appl Surf Sci*. 2011;257:10590–10594.

[30] Matykina E, Arrabal R, Skeldon P, et al. Transmission electron microscopy of coatings formed by plasma electrolytic oxidation of titanium. *Acta Biomat*. 2009;5:1356–1366.

[31] Rogov AB, Shayapov VR. The role of cathodic current in PEO of aluminum: influence of cationic electrolyte composition on the transient current-voltage curves and the discharges optical emission spectra. *Appl Surf Sci*. 2017;394:323–332.

[32] Venkateswarlu K, Rameshbabu N, Sreekanth D, et al. Role of electrolyte chemistry on electronic and in vitro electrochemical properties of micro-arc oxidized titania films on Cp Ti. *Electrochim Acta*. 2013;105:468–480.

[33] Simchen F, Sieber M, Lampke T. Electrolyte influence on ignition of plasma electrolytic oxidation processes on light metals. *Surf Coat Technol*. 2017;315:205–213.

[34] Ko YG, Namgung S, Shin DH. Correlation between KOH concentration and surface properties of AZ91 magnesium alloy coated by plasma electrolytic oxidation. *Surf Coat Technol*. 2010;205:2525–2531.

[35] Laleh M, Kargar F, Sabour Rouhaghdam A. Formation of a compact oxide layer on AZ91D magnesium alloy by microarc oxidation via addition of cerium chloride into the MAO electrolyte. *J Coat Technol Res*. 2011;8:765–771.

[36] Chen J, Wang Z, Lu S. Effects of electric parameters on microstructure and properties of MAO coating fabricated on ZK60 Mg alloy in dual electrolyte. *Rare Metals*. 2012;31:172–177.

[37] Tseng CC, Lee JL, Kuo TH, et al. The influence of sodium tungstate concentration and anodizing conditions on microarc oxidation (MAO) coatings for aluminum alloy. *Surf Coat Technol*. 2012;206:3437–3443.

[38] Wang SY, Xia YP, Liu L. Effects of sodium citrate on MAO process and characteristics of coatings fabricated on AZ91D magnesium alloy. In: Deng XC, Dong XF, editors. *Progress in new materials and*

mechanics research. Stafa-Zurich: Trans Tech Publications Ltd; 2012. p. 320–324.

[39] Martin J, Leone P, Nomine A, et al. Influence of electrolyte ageing on the plasma electrolytic oxidation of aluminium. Surf Coat Technol. 2015;269:36–46.

[40] Lu XP, Mohedano M, Blawert C, et al. Plasma electrolytic oxidation coatings with particle additions – a review. Surf Coat Technol. 2016;307:1165–1182.

[41] Arrabal R, Matykina E, Skeldon P, et al. Incorporation of zirconia particles into coatings formed on magnesium by plasma electrolytic oxidation. J Mater Sci. 2008;43:1532–1538.

[42] Li HX, Li WJ, Song RG, et al. Effects of different current densities on properties of MAO coatings embedded with and without a-Al2O3 nanoadditives. Mater Sci Technol. 2012;28:565–568.

[43] Lu XP, Blawert C, Kainer KU, et al. Investigation of the formation mechanisms of plasma electrolytic oxidation coatings on Mg alloy AM50 using particles. Electrochim Acta. 2016;196:680–691.

[44] Lu XP, Blawert C, Huang YD, et al. Plasma electrolytic oxidation coatings on Mg alloy with addition of SiO2 particles. Electrochim Acta. 2016;187:20–33.

[45] Fatimah S, Kamil MP, Kwon JH, et al. Dual incorporation of SiO2 and ZrO2 nanoparticles into the oxide layer on 6061 Al alloy via plasma electrolytic oxidation: coating structure and corrosion properties. J Alloys Compd. 2017;707:358–364.

[46] Wang P, Wu T, Xiao YT, et al. Effects of Al2O3 micro powder addition amount on characteristics of micro-arc oxidation coating formed on magnesium alloy. Rare Metal Mater Eng. 2017;46:1260–1264.

[47] Klapkiv M, Nykyforchyn H, Posuvailo V. Spectral analysis of an electrolytic plasma in the process of synthesis of aluminium oxide. Mater Sci. 1994;30:333–343.

[48] Klapkiv M. Simulation of synthesis of oxide-ceramic coatings in discharge channels of a metal-electrolyte system. Mater Sci. 1999;35:279–283.

[49] Klapkiv M, Chuchmarev O, Sydor P, et al. Thermodynamics of the interaction of aluminum, magnesium, and zirconium with components of an electrolytic plasma. Mater Sci. 2000;36:66–79.

[50] Dunleavy CS, Golosnoy IO, Curran JA, et al. Characterisation of discharge events during plasma electrolytic oxidation. Surf Coat Technol. 2009;203:3410–3419.

[51] Hussein RO, Nie X, Northwood DO, et al. Spectroscopic study of electrolytic plasma and discharging behaviour during the plasma electrolytic oxidation (PEO) process. J Phys D Appl Phys. 2010;43:Art. No. 105203.

[52] Jovovic J, Stojadinovic S, Sisovic NM, et al. Spectroscopic study of plasma during electrolytic oxidation of magnesium- and aluminium-alloy. J Quant Spectrosc Radiat Transfer. 2012;113:1928–1937.

[53] Wang L, Chen L, Yan Z, et al. Optical emission spectroscopy studies of discharge mechanism and plasma characteristics during plasma electrolytic oxidation of magnesium in different electrolytes. Surf Coat Technol. 2010;205:1651–1658.

[54] Stojadinovic S, Tadic N, Sisovic NM, et al. Real-time imaging, spectroscopy, and structural investigation of cathodic plasma electrolytic oxidation of molybdenum. J Appl Phys. 2015;117(23): Art. No.233304.

[55] Jovović J, Stojadinović S, Šišović NM, et al. Spectroscopic characterization of plasma during electrolytic oxidation (PEO) of aluminium. Surf Coat Technol. 2011;206:24–28.

[56] Sarvan M, Radic-Peric J, Kasalica B, et al. Investigation of long-duration plasma electrolytic oxidation of aluminum by means of optical spectroscopy. Surf Coat Technol. 2014;254:270–276.

[57] Dunleavy CS, Curran JA, Clyne TW. Self-similar scaling of discharge events through PEO coatings on aluminium. Surf Coat Technol. 2011;206:1051–1061.

[58] Hussein RO, Nie X, Northwood DO. A spectroscopic and microstructural study of oxide coatings produced on a Ti–6Al–4V alloy by plasma electrolytic oxidation. Mater Chem Phys. 2012;134:484–492.

[59] Dunleavy CS, Curran JA, Clyne TW. Time dependent statistics of plasma discharge parameters during bulk AC plasma electrolytic oxidation of aluminium. Appl Surf Sci. 2013;268:397–409.

[60] Nomine A, Troughton SC, Nomine AV, et al. High speed video evidence for localised discharge cascades during plasma electrolytic oxidation. Surf Coat Technol. 2015;269:125–130.

[61] Troughton SC, Nomine A, Nomine AV, et al. Synchronised electrical monitoring and high speed video of bubble growth associated with individual discharges during plasma electrolytic oxidation. Appl Surf Sci. 2015;359:405–411.

[62] Troughton SC, Nomine A, Dean J, et al. Effect of individual discharge cascades on the microstructure of plasma electrolytic oxidation coatings. Appl Surf Sci. 2016;389:260–269.

[63] Melhem A, Henrion G, Czerwiec T, et al. Changes induced by process parameters in oxide layers grown by the PEO process on Al alloys. Surf Coat Technol. 2011;205:S133–S1S6.

[64] Habazaki H, Tsunekawa S, Tsuji E, et al. Formation and characterization of wear-resistant PEO coatings formed on β-titanium alloy at different electrolyte temperatures. Appl Surf Sci. 2012;259:711–718.

[65] Martin J, Nominé A, Brochard F, et al. Delay in micro-discharges appearance during PEO of Al: evidence of a mechanism of charge accumulation at the electrolyte/oxide interface. Appl Surf Sci. 2017;410:29–41.

[66] Matykina E, Arrabal R, Pardo A, et al. Energy-efficient PEO process of aluminium alloys. Mater Lett. 2014;127:13–16.

[67] Curran JA, Clyne TW. Thermo-physical properties of plasma electrolytic oxide coatings on aluminium. Surf Coat Technol. 2005;199:168–176.

[68] Lee JH, Kim SJ. Effects of silicate ion concentration on the formation of ceramic oxide layers produced by plasma electrolytic oxidation on Al alloy. Jpn J Appl Phys. 2017;56(1):Art. No. 01AB01.

[69] Javidi M, Fadaee H. Plasma electrolytic oxidation of 2024-T3 aluminum alloy and investigation on microstructure and wear behavior. Appl Surf Sci. 2013;286:212–219.

[70] Xin SG, Song LX, Zhao RG, et al. Phase composition and properties of the micro-arc oxidation coating on aluminium matrix composite. J Inorg Mater. 2006;21:223–229.

[71] Friedemann AER, Gesing TM, Plagemann P. Electrochemical rutile and anatase formation on PEO surfaces. Surf Coat Technol. 2017;315:139–149.

[72] Ao N, Liu DX, Wang SX, et al. Microstructure and tribological behavior of a TiO$_2$/hBN composite ceramic coating formed via micro-arc oxidation of Ti-6Al-4V alloy. *J Mater Sci Technol.* 2016;32:1071–1076.

[73] Yerokhin AL, Leyland A, Matthews A. Kinetic aspects of aluminium titanate layer formation on titanium alloys by plasma electrolytic oxidation. *Appl Surf Sci.* 2002;200:172–184.

[74] Yao ZP, Liu YF, Xu YJ, et al. Effects of cathode pulse at high frequency on structure and composition of Al2TiO5 ceramic coatings on Ti alloy by plasma electrolytic oxidation. *Mater Chem Phys.* 2011;126:227–231.

[75] Curran JA, Clyne TW. Porosity in plasma electrolytic oxide coatings. *Acta Mater.* 2006;54:1985–1993.

[76] Yu XW, Chen L, Qin HL, et al. Formation process of in situ oxide coatings with high porosity using one-step plasma electrolytic oxidation. *Appl Surf Sci.* 2016;366:432–438.

[77] Zhang X, Aliasghari S, Nemcova A, et al. X-ray computed tomographic investigation of the porosity and morphology of plasma electrolytic oxidation coatings. *ACS Appl Mater Inter.* 2016;8:8801–8810.

[78] Shen MJ, Wang XJ, Zhang MF. High-compactness coating grown by plasma electrolytic oxidation on AZ31 magnesium alloy in the solution of silicate-borax. *Appl Surf Sci.* 2012;259:362–366.

[79] Zhang W, Tian B, Du KQ, et al. Preparation and corrosion performance of PEO coating with low porosity on magnesium alloy AZ91D in acidic KF system. *Int J Electrochem Sci.* 2011;6:5228–5248.

[80] Patel VK, Bhowmik S. Plasma processing of aluminum alloys to promote adhesion: a critical review. *Rev Adhes Adhes.* 2017;5:79–104.

[81] Dean J, Gu T, Clyne TW. Evaluation of residual stress levels in plasma electrolytic oxidation coatings using a curvature method. *Surf Coat Technol.* 2015;269:47–53.

[82] Aliofkhazraei M, Rouhaghdam AS. Fabrication of functionally gradient nanocomposite coatings by plasma electrolytic oxidation based on variable duty cycle. *Appl Surf Sci.* 2012;258:2093–2097.

[83] Krishna LR, Gupta P, Sundararajan G. The influence of phase gradient within the micro arc oxidation (MAO) coatings on mechanical and tribological behaviors. *Surf Coat Technol.* 2015;269:54–63.

[84] Arrabal R, Mota JM, Criado A, et al. Assessment of duplex coating combining plasma electrolytic oxidation and polymer layer on AZ31 magnesium alloy. *Surf Coat Technol.* 2012;206:4692–4703.

[85] Minaev AN, Gnedenkov SV, Sinebryukhov SL, et al. Composite coatings formed by plasma electrolytic oxidation. *Prot Met Phys Chem Surf.* 2011;47:840–849.

[86] Li Z, Jing X, Yuan Y, et al. Composite coatings on a Mg-Li alloy prepared by combined plasma electrolytic oxidation and sol-gel techniques. *Corros Sci.* 2012;63:358–366.

[87] Dunleavy CS, Curran JA, Clyne TW. Plasma electrolytic oxidation of aluminium networks to form a metal-cored ceramic composite hybrid material. *Comp Sci Tech.* 2011;71:908–915.

[88] Sabatini G, Ceschini L, Martini C, et al. Improving sliding and abrasive wear behaviour of cast A356 and wrought AA7075 aluminium alloys by plasma electrolytic oxidation. *Mater Des.* 2010;31:816–828.

[89] Cheng YL, Cao JH, Peng ZM, et al. Wear-resistant coatings formed on Zircaloy-2 by plasma electrolytic oxidation in sodium aluminate electrolytes. *Electrochim Acta.* 2014;116:453–466.

[90] Li QB, Liang J, Liu BX, et al. Effects of cathodic voltages on structure and wear resistance of plasma electrolytic oxidation coatings formed on aluminium alloy. *Appl Surf Sci.* 2014;297:176–181.

[91] Ma C, Zhang M, Yuan Y, et al. Tribological behavior of plasma electrolytic oxidation coatings on the surface of Mg8Li1Al alloy. *Tribol Int.* 2012;47:62–68.

[92] Treviño M, Garza-Montes-de-Oca NF, Párez A, et al. Wear of an aluminium alloy coated by plasma electrolytic oxidation. *Surf Coat Technol.* 2012;206:2213–2219.

[93] Khorasanian M, Dehghan A, Shariat MH, et al. Microstructure and wear resistance of oxide coatings on Ti-6Al-4V produced by plasma electrolytic oxidation in an inexpensive electrolyte. *Surf Coat Technol.* 2011;206:1495–1502.

[94] Aliofkhazraei M, Sabour Rouhaghdam A, Shahrabi T. Abrasive wear behaviour of Si$_3$N$_4$/TiO$_2$ nanocomposite coatings fabricated by plasma electrolytic oxidation. *Surf Coat Technol.* 2010;205:S41–SS6.

[95] Martini C, Ceschini L, Tarterini F, et al. PEO layers obtained from mixed aluminate–phosphate baths on Ti–6Al–4V: dry sliding behaviour and influence of a PTFE topcoat. *Wear.* 2010;269:747–756.

[96] Winter L, Morgenstern R, Hockauf K, et al. The effect of plasma electrolytic oxidation on the mean stress sensitivity of the fatigue life of the 6082 aluminum alloy. 18th Chemnitz Seminar on Materials Engineering. Bristol: IOP Publishing Ltd; 2016.

[97] Klein M, Lu X, Blawert C, et al. Influence of plasma electrolytic oxidation coatings on fatigue performance of AZ31 Mg alloy. *Mater Corros.* 2017;68:50–57.

[98] Kong DJ, Liu H, Wang JC. Effects of micro arc oxidation on fatigue limits and fracture morphologies of 7475 high strength aluminum alloy. *J Alloys Compd.* 2015;650:393–398.

[99] Němcová A, Skeldon P, Thompson GE, et al. Influence of plasma electrolytic oxidation on fatigue performance of AZ61 magnesium alloy. *Corros Sci.* 2014;82:58–66.

[100] Raman SGS, Rajasekaran B. Relative performance of alumina coatings prepared by micro arc oxidation and detonation Gun spray On AA 6063 under plain fatigue and fretting fatigue loading. *Trans Indian Inst Met.* 2008;61:465–471.

[101] Potomati F, Giordani EJ, Duarte LT, et al. Fatigue behavior and physical characterization of surface-modified Ti-6Al-4V ELI alloy by micro-arc oxidation. *Mater Res Ibero Am J Mater.* 2012;15:305–311.

[102] Khan RHU, Yerokhin AL, Pilkington A, et al. Residual stresses in plasma electrolytic oxidation coatings on Al alloy produced by pulsed unipolar current. *Surf Coat Technol.* 2005;200:1580–1586.

[103] Khan RHU, Yerokhin AL, Matthews A. Structural characteristics and residual stresses in oxide films produced on Ti by pulsed unipolar plasma electrolytic oxidation. *Philos Mag.* 2008;88:795–807.

[104] Shen D, Cai J, Guo C, et al. Evolution of residual stresses in micro-arc oxidation ceramic coatings on 6061 Al alloy. *Chinese J Mech Eng.* 2013;26:1149–1153.

[105] Asquith D, Yerokhin A, James N, et al. Evaluation of residual stress development at the interface of plasma

electrolytically oxidized and cold-worked aluminum. *Metall Mat Trans.* 2013;44A:4461–4465.

[106] Gu Y, Chen C, Bandopadhyay S, et al. Residual stress in pulsed dc microarc oxidation treated AZ31 alloy. *Surf Eng.* 2012;28:498–502.

[107] Wasekar NP, Jyothirmayi A, Krishna LR, et al. Effect of micro arc oxidation coatings on corrosion resistance of 6061-Al alloy. *J Mater Eng Perform.* 2008;17:708–713.

[108] Zhendong W, Zhaohua J, Zhongping Y, et al. Study on structure and corrosion resistance of micro arc oxidation black ceramic coatings on aluminum alloy. *Rare Metal Mater Eng.* 2007;36:687–689.

[109] Xu L, Ding JN, Xu XJ, et al. Wettability and corrosion resistance of ultrafine-grained titanium by micro-arc oxidation. *Rare Metal Mater Eng.* 2015;44:3100–3104.

[110] Hwang DY, Kim YM, Park DY, et al. Corrosion resistance of oxide layers formed on AZ91 Mg alloy in $KMnO_4$ electrolyte by plasma electrolytic oxidation. *Electrochim Acta.* 2009;54:5479–5485.

[111] Malayoglu U, Tekin KC, Shrestha S. Influence of post-treatment on the corrosion resistance of PEO coated AM50B and AM60B Mg alloys. *Surf Coat Technol.* 2010;205:1793–1798.

[112] Hussein RO, Northwood DO, Nie X. The effect of processing parameters and substrate composition on the corrosion resistance of plasma electrolytic oxidation (PEO) coated magnesium alloys. *Surf Coat Technol.* 2013;237:357–368.

[113] Mori Y, Koshi A, Liao J, et al. Characteristics and corrosion resistance of plasma electrolytic oxidation coatings on AZ31B Mg alloy formed in phosphate - silicate mixture electrolytes. *Corros Sci.* 2014;88:254–262.

[114] Krishna LR, Poshal G, Sundararajan G. Influence of electrolyte chemistry on morphology and corrosion resistance of micro arc oxidation coatings deposited on magnesium. *Metall Mater Trans A.* 2010;41A:3499–3508.

[115] Shen X, Nie X, Hu H, et al. Effects of coating thickness on thermal conductivities of alumina coatings and alumina/aluminum hybrid materials prepared using plasma electrolytic oxidation. *Surf Coat Technol.* 2012;207:96–101.

[116] Akatsu T, Kato T, Shinoda Y, et al. Thermal barrier coating made of porous zirconium oxide on a nickel-based single crystal superalloy formed by plasma electrolytic oxidation. *Surf Coat Technol.* 2013;223:47–51.

[117] Curran JA, Kalkanci H, Magurova Y, et al. Mullite-rich plasma electrolytic oxide coatings for thermal barrier applications. *Surf Coat Technol.* 2006;201:8683–8687.

[118] Shen DJ, Wang YL, Nash P, et al. Microstructure, temperature estimation and thermal shock resistance of PEO ceramic coatings on aluminum. *J Mater Process Technol.* 2008;205:477–481.

[119] Jiang YL, Wang JK, Hu B, et al. Preparation of a novel yellow ceramic coating on Ti alloys by plasma electrolytic oxidation. *Surf Coat Technol.* 2016;307:1297–1302.

[120] Wang S, Liu PC. The technology of preparing green coating by conducting micro-arc oxidation on AZ91D magnesium alloy. *Pol J Chem Technol.* 2016;18:36–40.

[121] Yang W, Wang JL, Xu DP, et al. Characterization and formation mechanism of grey micro-arc oxidation coatings on magnesium alloy. *Surf Coat Technol.* 2015;283:281–285.

[122] Shao ZC, Zhang QF, Yang L, et al. Preparation of dark-red membrane by micro-arc oxidation on AM50 alloys. *Mater Manuf Process.* 2015;30:1505–1509.

[123] Wang ZJ, Nie XY, Hu H, et al. In situ fabrication of blue ceramic coatings on wrought Al alloy 2024 by plasma electrolytic oxidation. *J Vac Sci Technol A.* 2012;30: Art. No. 021302.

[124] Dou Q, Li WF, Zhang GG, et al. Preparation and characterisation of black ceramic coating on AZ91D magnesium alloy by plasma electrolytic oxidation with reduced energy consumption. *Mater Res Innov.* 2015;19(Suppl. 2). doi:10.1179/1432891715Z.0000000001309

[125] Hwang IJ, Shin KR, Lee JS, et al. Formation of black ceramic layer on aluminum alloy by plasma electrolytic oxidation in electrolyte containing Na_2WO_4. *Mater Trans.* 2012;53:559–564.

[126] Li K, Li WF, Zhang GG, et al. Preparation of black PEO layers on Al-Si alloy and the colorizing analysis. *Vacuum.* 2015;111:131–136.

[127] Jin FY, Wang K, Zhu M, et al. Infrared reflection by alumina films produced on aluminum alloy by plasma electrolytic oxidation. *Mater Chem Phys.* 2009;114:398–401.

[128] Dicu M, Matei A, Abrudeanu M, et al. Synthesis and properties of the porous titania coatings formed on titanium by plasma electrolytic oxidation for biomedical application. *J Optoelectron Adv Mater.* 2011;13:324–331.

[129] Koegler WS, Griffith LG. Osteoblast response to PLGA tissue engineering scaffolds with PEO modified surface chemistries and demonstration of patterned cell response. *Biomaterials.* 2004;25:2819–2830.

[130] Whiteside P, Matykina E, Gough JE, et al. In vitro evaluation of cell proliferation and collagen synthesis on titanium following plasma electrolytic oxidation. *J Biomed Mater Res A.* 2010;94:38–46.

[131] Robinson HJ, Markaki AE, Collier CA, et al. Cell adhesion to plasma electrolytic oxidation (PEO) titania coatings, assessed using a centrifuging technique. *J Mech Behav Biomed Mater.* 2011;4:2103–2112.

[132] Siu HT, Man HC. Fabrication of bioactive titania coating on nitinol by plasma electrolytic oxidation. *Appl Surf Sci.* 2013;274:181–187.

[133] Hornberger H, Virtanen S, Boccaccini AR. Biomedical coatings on magnesium alloys - a review. *Acta Biomat.* 2012;8:2442–2455.

[134] Mohedano M, Luthringer BJC, Mingo B, et al. Bioactive plasma electrolytic oxidation coatings on Mg-Ca alloy to control degradation behaviour. *Surf Coat Technol.* 2017;315:454–467.

[135] Tang H, Han Y, Wu T, et al. Synthesis and properties of hydroxyapatite-containing coating on AZ31 magnesium alloy by micro-arc oxidation. *Appl Surf Sci.* 2017;400:391–404.

[136] Yao ZP, Li LL, Jiang ZH. Adjustment of the ratio of Ca/P in the ceramic coating on Mg alloy by plasma electrolytic oxidation. *Appl Surf Sci.* 2009;255:6724–6728.

[137] Gu XN, Li N, Zhou WR, et al. Corrosion resistance and surface biocompatibility of a microarc oxidation coating on a Mg-Ca alloy. *Acta Biomat.* 2011;7:1880–1889.

[138] Zhang L, Zhang JQ, Chen CF, et al. Advances in microarc oxidation coated AZ31 Mg alloys for biomedical applications. *Corros Sci.* 2015;91:7–28.

[139] Akpan UG, Hameed BH. Parameters affecting the photocatalytic degradation of dyes using TiO_2-based photocatalysts: a review. *J Hazard Mater.* 2009;170:520–529.

[140] Awazu K, Fujimaki M, Rockstuhl C, et al. A plasmonic photocatalyst consisting of sliver nanoparticles embedded in titanium dioxide. *J Am Chem Soc.* 2008;130:1676–1680.

[141] Shin YK, Chae WS, Song YW, et al. Formation of titania photocatalyst films by microarc oxidation of Ti and Ti–6Al–4V alloys. *Electrochem Commun.* 2006;8:465–470.

[142] Akatsu T, Yamada Y, Hoshikawa Y, et al. Multifunctional porous titanium oxide coating with apatite forming ability and photocatalytic activity on a titanium substrate formed by plasma electrolytic oxidation. *Mater Sci Eng C-Mater.* 2013;33:4871–4875.

[143] He J, Luo Q, Cai QZ, et al. Microstructure and photocatalytic properties of WO_3/TiO_2 composite films by plasma electrolytic oxidation. *Mater Chem Phys.* 2011;129:242–248.

[144] Bayati MR, Golestani-Fard F, Moshfegh AZ. How photocatalytic activity of the MAO-grown TiO_2 nano/micro-porous films is influenced by growth parameters? *Appl Surf Sci.* 2010;256:4253–4259.

[145] Mizukoshi Y, Ohtsu N, Semboshi S, et al. Visible light responses of sulfur-doped rutile titanium dioxide photocatalysts fabricated by anodic oxidation. *Appl Catal B Environ.* 2009;91:152–156.

[146] Oh H-J, Chi C-S. Eu–N-doped TiO_2 photocatalyst synthesized by micro-arc oxidation. *Mater Lett.* 2012;86:31–33.

[147] Coto M, Troughton SC, Duan J, et al. Development and assessment of photo-catalytic membranes for water purification using solar radiation. *Appl Surf Sci.* 2018;433:101–107.

[148] Luttrell T, Halpegamage S, Tao J, et al. Why is anatase a better photocatalyst than rutile? - model studies on epitaxial TiO_2. *Sci Rep.* 2014;4:4043.

[149] Mirelman LK, Curran JA, Clyne TW. The production of anatase-rich photoactive coatings by plasma electrolytic oxidation. *Surf Coat Technol.* 2012;207:66–71.

[150] Reed T. *Free energy of formation of binary compounds.* Cambridge (MA): MIT Press; 1971.

[151] Stull DR, Prophet H. JANAF Thermochemical Tables, NSRDS-NBS 37: US Dept of Commerce, National Bureau of Standards; 1971.

[152] Wang YL, Jiang ZH, Yao ZP. Microstructure, bonding strength and thermal shock resistance of ceramic coatings on steels prepared by plasma electrolytic oxidation. *Appl Surf Sci.* 2009;256:650–656.

[153] Wang YL, Jiang ZH, Yao ZP. Preparation and properties of ceramic coating on Q235 carbon steel by plasma electrolytic oxidation. *Curr Appl Phys.* 2009;9:1067–1071.

[154] Yerokhin AL, Lyubimov VV, Ashitkov RV. Phase formation in ceramic coatings during plasma electrolytic oxidation of aluminium alloys. *Ceram Int.* 1998;24:1–6.

[155] Charlu TV, Kleppa OJ, Reed TB. High temperature combustion calorimetry 3. Enthalpies of formation of titanium oxides. *J Chem Thermodyn.* 1974;6:1065–1074.

[156] Matykina E, Arrabal R, Skeldon P, et al. Plasma electrolytic oxidation of a zirconium alloy under AC conditions. *Surf Coat Technol.* 2010;204:2142–2151.

[157] Sandhyarani M, Rameshbabu N, Venkateswarlu K, et al. Surface morphology, corrosion resistance and in vitro bioactivity of P containing $ZrO2$ films formed on Zr by plasma electrolytic oxidation. *J Alloys Compd.* 2013;553:324–332.

[158] Apelfeld AV, Borisov AM, Krit BL, et al. The study of plasma electrolytic oxidation coatings on Zr and Zr-1% Nb alloy at thermal cycling. *Surf Coat Technol.* 2015;269:279–285.

[159] He SX, Ma YL, Ye H, et al. Ceramic oxide coating formed on beryllium by micro-arc oxidation. *Corros Sci.* 2017;122:108–117.

[160] Urbahs A, Urbaha M, Zujevs V, et al. *Composition and structure of micro arc oxidation coatings. Transport means 2013.* Kaunas: Kaunas University Technology Press; 2013, p. 101–105.

[161] Lu LH, Zhang JW, Shen DJ. Characterization of anatase coatings on NiTi shape memory alloy by plasma electrolytic oxidation method. In: Sun D, Sung WP, Chen R, editors. *Frontiers of manufacturing and design science Ii, Pts 1-6.* Stafa-Zurich: Trans Tech Publications Ltd; 2012. p. 3837–3841.

[162] Rudnev VS, Boguta DL, Yarovaya TP, et al. Coatings based on niobium oxides and phosphates formed on niobium alloy. *Prot Metals Phys Chem Surf.* 2014;50:360–362.

[163] Sowa M, Kazek-Kesik A, Krzakala A, et al. Modification of niobium surfaces using plasma electrolytic oxidation in silicate solutions. *J Solid State Electrochem.* 2014;18:3129–3142.

[164] Stojadinovic S, Tadic N, Radic N, et al. Anodic luminescence, structural, photoluminescent, and photocatalytic properties of anodic oxide films grown on niobium in phosphoric acid. *Appl Surf Sci.* 2015;355:912–920.

[165] Sowa M, Worek J, Dercz G, et al. Surface characterisation and corrosion behaviour of niobium treated in a Ca- and P-containing solution under sparking conditions. *Electrochim Acta.* 2016;198:91–103.

[166] Stojadinovic S, Vasilic R. Orange-red photoluminescence of $Nb2O5$: Eu3+, Sm3+ coatings formed by plasma electrolytic oxidation of niobium. *J Alloys Compd.* 2016;685:881–889.

[167] Ge YL, Wang YM, Zhang YF, et al. The improved thermal radiation property of SiC doped microarc oxidation ceramic coating formed on niobium metal for metal thermal protective system. *Surf Coat Technol.* 2017;309:880–886.

[168] Sowa M, Kazek-Kesik A, Socha RP, et al. Modification of tantalum surface via plasma electrolytic oxidation in silicate solutions. *Electrochim Acta.* 2013;114:627–636.

[169] Stojadinovic S, Vasilic R, Peric M. Investigation of plasma electrolytic oxidation on valve metals by means of molecular spectroscopy – a review. *RSC Adv.* 2014;4:25759–25789.

[170] Michaelis A. Valve metal, Si and ceramic oxides as dielectric films for passive and active electronic devices. In: Alkire R, Kolb D, Lipkowski J, Ross P, editors. *Advances in electrochemical science and engineering*, vol. 10. Weinheim: Wiley; 2008. p. 1–106.

[171] Tuckerman ME, Chandra A, Marx D. Structure and dynamics of OH-(aq). *Accounts Chem Res.* 2006;39:151–158.

[172] Nominé A, Nominé AV, Braithwaite NS, et al. High-frequency induced cathodic breakdown during plasma electrolytic oxidation. *Appl Phys Lett*. 2017;8(3). Art. No. 031001. doi:10.1103/PhysRevApplied.8.031001.

[173] Strehlow W, Cook E. Compilation of energy band gaps in elemental and binary compound semiconductors and insulators. *J Phys Chem Ref Data*. 2009;2:163–199.

[174] Fromhold AT, Cook EL. Kinetics of oxide film growth on metal crystals – electron tunneling and ionic diffusion. *Phys Rev*. 1967;158:600.

[175] Munoz AG, Bessone JB. Anodic oxide growth on aluminium surfaces modified by cathodic deposition of Ni and Co. *Thin Solid Films*. 2004;460:143–149.

[176] Robertson J. High dielectric constant gate oxides for metal oxide Si transistors. *Rep Prog Phys*. 2006;69:327–396.

[177] Ono S, Moronuki S, Mori Y, et al. Effect of electrolyte concentration on the structure and corrosion resistance of anodic films formed on magnesium through plasma electrolytic oxidation. *Electrochim Acta*. 2017;240:415–423.

[178] Yahalom J, Zahavi J. Experimental evaluation of some electrolytic breakdown hypotheses. *Electrochim Acta*. 1971;16:603.

[179] Ikonopisov S, Girginov A, Machkova M. Electrical breaking down of barrier anodic films during their formation. *Electrochim Acta*. 1979;24:451–456.

[180] Klein N, Moscovici V, Kadary V. Electrical breakdown during the anodic growth of aluminium oxide. *J Electrochem Soc*. 1980;127:152–155.

[181] Kadary V, Klein N. Electrical breakdown during the anodic growth of tantalum pentoxide. *J Electrochem Soc*. 1980;127:139–151.

[182] Nie X, Meletis E, Jiang J, et al. Abrasive wear/corrosion properties and TEM analysis of Al2O3 coatings fabricated using plasma electrolysis. *Surf Coat Technol*. 2002;149:245–251.

[183] Monfort F, Berkani A, Matykina E, et al. Development of anodic coatings on aluminium under sparking conditions in silicate electrolyte. *Corros Sci*. 2007;49:672–693.

[184] Arrabal R, Matykina E, Hashimoto T, et al. Characterization of AC PEO coatings on magnesium alloys. *Surf Coat Technol*. 2009;203:2207–2220.

[185] Tillous K, Toll-Duchanoy T, Bauer-Grosse E, et al. Microstructure and phase composition of microarc oxidation surface layers formed on aluminium and its alloys 2214-T6 and 7050-T74. *Surf Coat Technol*. 2009;203:2969–2973.

[186] Kasalica B, Radic-Peric J, Peric M, et al. The mechanism of evolution of microdischarges at the beginning of the PEO process on aluminum. *Surf Coat Technol*. 2016;298:24–32.

[187] Vol'f E, Sizikov A, Bugaenko L. Determination of the mean lifetime of vapor-plasma bubbles for a microdischarge on aluminum valve anode in aqueous electrolyte solution. *High Energ Chem*. 1998;32:407–410.

[188] Wang L, Fu W, Chen L. Evolution of active species and discharge sparks in Na_2SiO_3 electrolyte during PEO process. *J Alloys Compd*. 2011;509:7652–7656.

[189] Hamdan A, Noel C, Kosior F, et al. Dynamics of bubbles created by plasma in heptane for micro-gap conditions. *J Acoust Soc Am*. 2013;134:991–1000.

[190] Sengupta SK, Srivastava AK, Singh R. Contact glow discharge electrolysis: a study on its origin in the light of the theory of hydrodynamic instabilities in local solvent vaporisation by joule heating during electrolysis. *J Electroanal Chem*. 1997;427:23–27.

[191] Sengupta SK, Singh R, Srivastava AK. A study on the origin of nonfaradaic behavior of anodic contact glow discharge electrolysis – the relationship between power dissipated in glow discharges and nonfaradaic yields. *J Electrochem Soc*. 1998;145:2209–2213.

[192] Snizhko LO, Yerokhin AL, Gurevina NL, et al. Excessive oxygen evolution during plasma electrolytic oxidation of aluminium. *Thin Solid Films*. 2007;516:460–464.

[193] Conway BE, Tilak BV. Interfacial processes involving electrocatalytic evolution and oxidation of H-2, and the role of chemisorbed H. *Electrochim Acta*. 2002;47:3571–3594.

[194] Xin SG, Song LX, Zhao RG, et al. Influence of cathodic current on composition, structure and properties of Al2O3 coatings on aluminum alloy prepared by micro-arc oxidation process. *Thin Solid Films*. 2006;515:326–332.

[195] Wang JH, Du MH, Han FZ, et al. Effects of the ratio of anodic and cathodic currents on the characteristics of micro-arc oxidation ceramic coatings on Al alloys. *Appl Surf Sci*. 2014;292:658–664.

[196] Rakoch AG, Gladkova AA, Linn Z, et al. The evidence of cathodic micro-discharges during plasma electrolytic oxidation of light metallic alloys and micro-discharge intensity depending on pH of the electrolyte. *Surf Coat Technol*. 2015;269:138–144.

[197] Sah SP, Tsuji E, Aoki Y, et al. Cathodic pulse breakdown of anodic films on aluminium in alkaline silicate electrolyte – understanding the role of cathodic half-cycle in AC plasma electrolytic oxidation. *Corros Sci*. 2012;55:90–96.

[198] Nomine A, Martin J, Henrion G, et al. Effect of cathodic micro-discharges on oxide growth during plasma electrolytic oxidation (PEO). *Surf Coat Technol*. 2015;269:131–137.

[199] Fatkullin AR, Parfenov EV, Yerokhin A, et al. Effect of positive and negative pulse voltages on surface properties and equivalent circuit of the plasma electrolytic oxidation process. *Surf Coat Technol*. 2015;284:427–437.

[200] Rogov AB, Yerokhin A, Matthews A. The role of cathodic current in plasma electrolytic oxidation of aluminum: phenomenological concepts of the "soft sparking" mode. *Langmuir*. 2017;33:11059–11069.

[201] Wang HY, Zhu RF, Lu YP, et al. Preparation and mechanism of controllable micropores on bioceramic TiO2 coatings by plasma electrolytic oxidation. *Surf Rev Lett*. 2013;20(5). Art. No. 1350051. doi:10.1142/S0218625X13500510.

[202] Zou B, Lu GH, Zhang GL, et al. Effect of current frequency on properties of coating formed by microarc oxidation on AZ91D magnesium alloy. *Trans Nonferrous Metals Soc China*. 2015;25:1500–1505.

[203] Yerokhin AL, Shatrov A, Samsonov V, et al. Oxide ceramic coatings on aluminium alloys produced by a pulsed bipolar plasma electrolytic oxidation process. *Surf Coat Technol*. 2005;199:150–157.

[204] Yerokhin A, Parfenov EV, Matthews A. In situ impedance spectroscopy of the plasma electrolytic oxidation process for deposition of Ca- and P-containing, coatings on Ti. *Surf Coat Technol*. 2016;301:54–62.

[205] Jaspard-Mécuson F, Czerwiec T, Henrion G, et al. Tailored aluminium oxide layers by bipolar current adjustment in the plasma electrolytic oxidation (PEO) process. *Surf Coat Technol*. 2007;201:8677–8682.

[206] Slonova AI, Terleeva OP. Morphology, structure, and phase composition of microplasma coatings formed on Al-Cu-Mg alloy. *Protect Metals.* 2008;44:65–75.

[207] Matykina E, Arrabal R, Mohamed A, et al. Plasma electrolytic oxidation of pre-anodized aluminium. *Corros Sci.* 2009;51:2897–2905.

[208] Matykina E, Arrabal R, Skeldon P, et al. AC PEO of aluminium with porous alumina precursor films. *Surf Coat Technol.* 2010;205:1668–1678.

[209] Matykina E, Arrabal R, Scurr DJ, et al. Investigation of the mechanism of plasma electrolytic oxidation of aluminium using O-18 tracer. *Corros Sci.* 2010;52:1070–1076.

[210] Gebarowski W, Pietrzyk S. Influence of the cathodic pulse on the formation and morphology of oxide coatings on aluminium produced by plasma electrolytic oxidation. *Arch Metall Mater.* 2013;58:241–245.

[211] Kamil MP, Kaseem M, Ko YG. Soft plasma electrolysis with complex ions for optimizing electrochemical performance. *Sci Rep.* 2017;7. Art. No. 4458. doi:10.1038/srep44458.

[212] Tjiang F, Ye L-W, Huang Y-J, et al. Effect of processing parameters on soft regime behavior of plasma electrolytic oxidation of magnesium. *Ceram Int.* 2017;43:S567–SS72.

[213] Cheng YL, Wang T, Li SX, et al. The effects of anion deposition and negative pulse on the behaviours of plasma electrolytic oxidation (PEO)-a systematic study of the PEO of a zirlo alloy in aluminate electrolytes. *Electrochim Acta.* 2017;225:47–68.

[214] Mohedano M, Matykina E, Arrabal R, et al. PEO of rheocast A356 Al alloy: energy efficiency and corrosion properties. *Surf Interface Anal.* 2016;48:953–959.

[215] Matykina E, Arrabal R, Mohedano M, et al. Recent advances in energy efficient PEO processing of aluminium alloys. *Trans Nonferrous Metals Soc China.* 2017;27:1439–1454.

[216] Zhang XM, Tian XB, Yang SQ, et al. Low energy-consumption plasma electrolytic oxidation based on grid cathode. *Rev Sci Instrum.* 2010;81(10). Art. No. 103504. doi:10.1063/1.3500319.